Available online at www.sciencedirect.com

ScienceDirect

Geochimica et Cosmochimica Acta xxx (2022) xxx–xxx

Geochimica et Cosmochimica Acta

www.elsevier.com/locate/gca

Chemical weathering signatures at Mt. Achernar, Central Transantarctic Mountains II: Surface exposed sediments

Joseph A Graly [a,b,*], Kathy J Licht [b], Nicole A Bader [b], Christine M Kassab [b], David L Bish [c], Michael R Kaplan [d]

[a] *Northumbria University, Geography and Environmental Sciences, Newcastle Upon Tyne, UK*
[b] *Indiana University Purdue University Indianapolis, Earth Sciences, Indianapolis, IN, USA*
[c] *Indiana University, Earth and Atmospheric Sciences, Bloomington, IN, USA*
[d] *Lamont-Doherty Earth Observatory, Palisades, NY, USA*

Received 1 October 2021; accepted in revised form 16 June 2022; available online xxxx

Abstract

Mt Achernar Moraine is a high altitude, high latitude blue ice moraine where typical conditions preclude the presence of liquid water. Cosmogenic and salt accumulation dating indicate that the moraine's surface is progressively older away from the active ice margin, with surface exposure ages up to 1 Ma. We analyze the chemical and mineralogical transformations in the <63 μm fraction along transects across the moraine. Data include bulk chemical composition, crystalline mineralogy by X-ray diffraction (XRD), and the composition of amorphous or low abundance products of chemical weathering by sequential extraction. These data are analyzed by multiple regression as a function of exposure age and as a function of composition of the moraine's cobble and pebble-sized clasts. Change with exposure age is defined by the development of salts and carbonate minerals along with the input of detrital material, principally from sedimentary rocks. Clay minerals and amorphous cements breakdown as detrital material in proportions far above their abundance in the rock clasts, whereas framework silicates (i.e. feldspars and quartz) break down in relatively small proportions. Both the carbonate minerals and some of the salts form from atmospheric acids (i.e. H_2CO_3) that in turn react with other minerals. Mass balance shows that the input of these atmospheric acids balances with gains in authigenic smectites, zeolites, and amorphous material. Many of these minerals also form in the subglacial environment, but are poorly represented in the underlying rock, suggesting a similar chemical weathering regime in both the subglacial and surface environments of this hyper cold and arid setting. The rate of CO_2 drawdown into carbonate minerals increases as the moraine progressively thickens, from 3 $mg{\cdot}m^2{\cdot}a^{-1}$ in freshly emerging sediments to ~50 $mg{\cdot}m^2{\cdot}a^{-1}$ after 500 ka of exposure. Weathering from acidic aerosols is proportional to atmospheric flux documented in ice cores and does not vary with moraine thickness. The carbonate mineral formation rates are more than an order of magnitude below those of the subglacial environment and as much as two orders of magnitude below those found in warm desert soils. Nevertheless, the drawdown of atmospheric CO_2 into carbonate minerals occurs in a terrestrial setting where water exists only in vapor form.

Keywords: Antarctica; Chemical weathering; Clay minerals; Carbonate minerals; Salts; Geochemical cycles

1. INTRODUCTION

Much of the aerially exposed landscape of Antarctica has a distinctly weathered character, with visibly oxidized and pitted surfaces, and extensive deposits of atmosphere-

* Corresponding author.
E-mail address: Joseph.graly@northumbria.ac.uk (J.A Graly).

https://doi.org/10.1016/j.gca.2022.06.024
0016-7037/© 2022 Published by Elsevier Ltd.

derived salts. Through much of the continent, soils have been characterized primarily by the development of salts, along with Fe oxidation and physical weathering (Bockheim, 1997). Past studies of chemical weathering under Antarctic surface conditions have suggested some authigenic formation of soil minerals (such as clay minerals) but with significant detrital input of clays from the breakdown of micas in the source rocks (Claridge and Campbell, 1984; Vennum and Nejedly, 1990). Few studies have offered quantitative rates of physical and chemical alteration on Antarctica's non-glaciated surfaces. And rates of atmospheric gas drawdown into the chemical weathering products of these soils have not been previously assessed.

Here we report the changes in geochemistry and mineralogy of the fine sediment in progressively older surface-exposed deposits of an Antarctic blue ice moraine. The site, Mt. Achernar Moraine, is located in the central Transantarctic Mountains, adjacent to the polar plateau. The companion to this paper compared Mt. Achernar Moraine's freshly emerging subglacial sediments to the underlying rock (Graly et al., 2020). We found that the subglacial sediment was substantially enriched in chemical weathering products, particularly smectite, kaolinite, and carbonate minerals and argued that air bubbles in the ice melt were driving the chemical transformations. Our objective here is to compare both the type and rate of mineral transformations on the moraine surface in contrast to the water-rich but atmosphere-limited subglacial environment.

1.1. Field Site

Mt. Achernar Moraine is cold and dry even by Antarctic standards. Mean annual precipitation is ~4 $cm{\cdot}a^{-1}$ (Bockheim, 1990; Scarrow et al., 2014), average annual temperature is −39 °C (Van Wessem et al., 2014), and average summer high temperature is the order of −15 °C (Comiso, 2000). Snowfall is lost almost entirely through sublimation or wind scouring and conditions with liquid water above 0 °C are rare. Melt is observed a few days a year at the moraine margin, where the dark sediment is thin enough to diffuse direct solar radiation as heat to the ice below, even under subzero conditions. However, melt pond features are absent once the sediment reaches 2–3 cm thickness (Bader et al., 2017), and melt of snow or clean ice has not been observed. Furthermore, the distribution of salts in the moraine strongly suggests against even rare flow through porous media events, with highly soluble salts accumulating linearly with exposure age on the moraine surface and only salts whose antecedent acids have relatively high vapor pressures at low temperatures occurring at depth (Graly et al., 2018b).

As a blue ice moraine, Mt. Achernar Moraine differs from typical glacial moraines in that the entire moraine is underlain by >150 m of debris-laden glacier ice and even the oldest portions still accumulate ice-entrained debris from depth via sublimation (Kassab et al., 2020). As a result, the till becomes progressively thicker with time (Graly et al., 2018c; Scarrow et al., 2014). New sediments accumulate at the bottom of the sediment column and, barring overturning, the sediments on the surface of the moraine are the oldest and longest exposed (Kaplan et al., 2017). Soil profile characterization suggests that, at least on the tops of the moraine's ridges, atmosphere-deposited salts and chemical weathering products remain within the topsoil and cryoturbation has not disturbed the soil structure (Graly et al., 2018b; Scarrow et al., 2014).

The moraine's structure is known both from surface morphology (Bader et al., 2017) and ground-penetrating radar (GPR) transects that reveal debris bands extending to depth (Kassab et al., 2020). Most of the moraine consists of a series of ridges and troughs that are generally subparallel to the ice margin of Law Glacier. Bader and others (2017) divided the morphology of the moraine into five zones that increase in age away from the glacier terminus: Zone 1 consists primarily of hummocky terrain, with hills dissected by melt ponds; Zone 2 is a small relatively flat-lying area behind Zone 1; Zone 3 consists of large (~10 m tall), broad (~100 m across) ridges; Zone 4 consists of much shorter, steeper, continuous ridges; Zone 5 is relatively flat lying, with visible structures mirroring the morphology of the ice tongues that flow over the mountains behind the moraine (Fig. 1). We consider debris-rich portions of Law Glacier's surface to be Zone 0. The GPR transects suggest that in Zones 1–3, subglacial material is fed to the surface by bands of ice-bound debris traced towards the ice-rock interface (Kassab et al., 2020). In Zone 4, distinct bands are not detectable in the radar transects, which suggests an increased abundance of subglacial debris.

Throughout the moraine, the pebble and cobble-sized clasts are characteristic of the Lower Beacon Supergroup and the Ferrar Dolerite (Bader et al., 2017), which outcrop in this region of the central Transantarctic Mountains (Faure and Mensing, 2010). Derivation of the moraine's material from the Lower Beacon Supergroup (below Upper Buckley) is confirmed by detrital zircon analysis (Bader et al., 2017). However, portions of the moraine differ dramatically in the relative abundance of these rock types. In freshly emerging sediments (Zone 1) and in the older portions (Zones 4 & 5) of the moraine, sedimentary and metasedimentary rock derived from the Lower Beacon Supergroup represent ~40% of clasts and ~60% of the clasts are derived from the Ferrar Dolerite. In the middle sections of the moraine (Zones 2 & 3), sedimentary and metasedimentary rock abundance in the pebble and cobble fraction rises to ~70% (Bader et al., 2017). Within Zone 4, there are also discrete bands enriched in sedimentary and metasedimentary rock. These counts of cobble clasts do not fully characterize bedrock input across all sediment size fractions. In the <63 μm fraction of freshly emerging sediments in Zones 0 and 1, the composition of elements and minerals not subject to major chemical or physical changes in the subglacial environment was consistent with an only ~30% contribution of Ferrar Dolerite and ~70% contribution from Beacon Supergroup rocks, which is half the abundance of Ferrar Dolerite found in the pebble size fraction (Graly et al., 2020). This implies that the less friable dolerite is enriched in the pebble fraction compared to its contribution to the <63 μm fraction.

The chronology of moraine formation at the site has been well-described with cosmogenic isotopes (Hagen,

Please cite this article in press as: Graly J. A., et al. Chemical weathering signatures at Mt. Achernar, Central Transantarctic Mountains II: Surface exposed sediments. *Geochim. Cosmochim. Acta* (2022), https://doi.org/10.1016/j.gca.2022.06.024

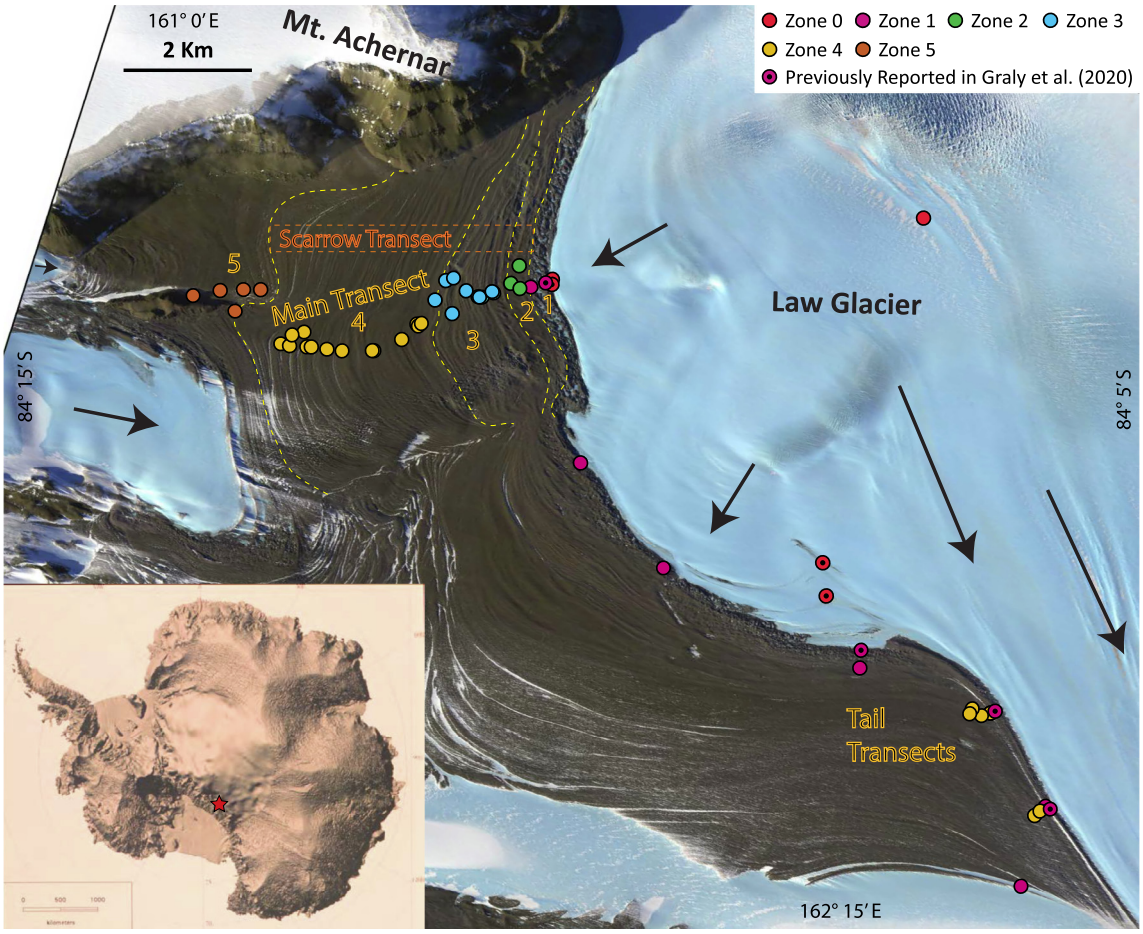

Fig. 1. Sampling locations on Mt. Achernar Moraine, Central Transantarctic Mountains. The main transect is divided into geomorphic zones (numbers labelled) per Bader et al. (2017). The approximate location of the transect collected by Scarrow et al. (2014) is also shown. Approximate down glacier flowlines illustrated with arrows and flow into the moraine. Imagery courtesy of U.S. Polar Geospatial Center.

1995; Kaplan et al., 2017) as well as with the salt chemistry of sediment samples (Graly et al., 2018b). The cosmogenic isotopes suggest little or no previous exposure in freshly emerging rocks and document moraine formation during the past 500,000 years. Salt development suggests that the oldest, undated portions of the moraine could have up to 1,000,000 years of surface exposure (Graly et al., 2018b). This record allows us to assess chemical effects of subaerial exposure in a hyper-arid and almost perpetually frozen environment.

2. METHODS

2.1. Field Sampling

Fifty-eight samples were collected from Mt. Achernar Moraine and the adjoining glacial surface, 36 during 2010 and 22 during 2015 (Fig. 1). The sampled sites range from water-saturated, freshly emerging sediment to till with over 1 Ma of salt accumulation (Fig. 2). Of these, 39 samples fall along a single transect through the widest part of the moraine. We refer to these samples as the Main Transect. The other 19 samples were taken from down-glacier sections of the moraine. This includes two short transects into a portion of the moraine we refer to as the Tail. This region is characterized by a tall lateral moraine separated by a linear depression from the visibly oxidized juxtaposed sediments beyond (Fig. 2). In addition to these transects, five samples were collected at isolated locations near the glacial edge of the moraine. An additional three samples were collected at debris-bearing bands on the surface of Law Glacier (well away from the moraine proper) (Fig. 1). Salt content data for the Main Transect samples were previously reported in Graly et al. (2018b).

Sediment samples were collected by shoveling material with an inert plastic scoop into plastic bags. Where thickness was sufficient, the top 2–3 cm were removed to avoid the presumed wind-deflation layer. At a few sites, samples were taken above and below distinct chromatic horizons, or from adjoining ridges and troughs. Otherwise, material was collected from within the top 5 cm of the soil profile along the broad crests characteristic of the moraine, where sediment is thickest and geomorphic overturning thought to be minimal (Graly et al., 2018b; Kassab et al., 2020). At 26 of the sampling sites, an adjoining pebble and cobble sample was collected, representing the clasts ranging from ~40 to ~100 mm diameter present within a square meter surface area. The clast petrology and grain size analyses for the 36

Please cite this article in press as: Graly J. A., et al. Chemical weathering signatures at Mt. Achernar, Central Transantarctic Mountains II: Surface exposed sediments. *Geochim. Cosmochim. Acta* (2022), https://doi.org/10.1016/j.gca.2022.06.024

Fig. 2. Photographs of characteristic sections of the moraine. (A) Freshly emerging Zone 0 sediments on Law Glacier (GPS for scale). (B) Zone 1 dissected by characteristic melt ponds; boulders are on an ~1 m scale. (C) ~10–20 ka old sediments forming a ridge in Zone 3. (D) Order of 500 ka old sediments from the back of Zone 4 showing high oxidized boulders and sediment white from salts (ice axe for scale). (E) Zone 5, which by the boron proxy, contains the oldest sediments in the moraine. (F) The tail section of the moraine with a tall ridge characteristic of Zone 1 juxtaposed against highly weathered sediments characteristic of Zone 4.

sediment samples collected in 2010 are reported in Bader et al. (2017).

2.2. Laboratory Analyses

Mineralogical and chemical analyses were performed on the <63 μm fraction, where products of chemical alteration are most likely to form. Traditional methods of assessing chemical weathering, such as chemical index of alteration (Nesbitt and Young, 1982), depend on the leaching of mobile elements from the soil system, resulting in the increasing abundance of immobile elements in the remaining sediments. In our ultra-arid field site, chemically leached elements cannot leave the site through groundwater or surface-water and will instead accumulate in the finest grain fractions. We therefore expect to see inverted results from a chemical index of alteration analysis, with older, weathered samples showing higher proportions of mobile elements and lower proportions of immobile elements in the <63 μm fraction.

In the <1000 μm fraction, grain size was measured in sediments dispersed with $Na_6(PO_3)_6$ by Malvern Mastersizer 2000. For geochemical analyses, one g aliquots of dry-sieved, <63 μm material from each sample were analyzed in a sequence of progressively stronger chemical extractions (Tessier et al., 1979; Ure and Davidson, 2002). Our extraction isolates water-soluble minerals such as salts and sulfates, 0.11 M acetic acid (CH_3COOH) – soluble

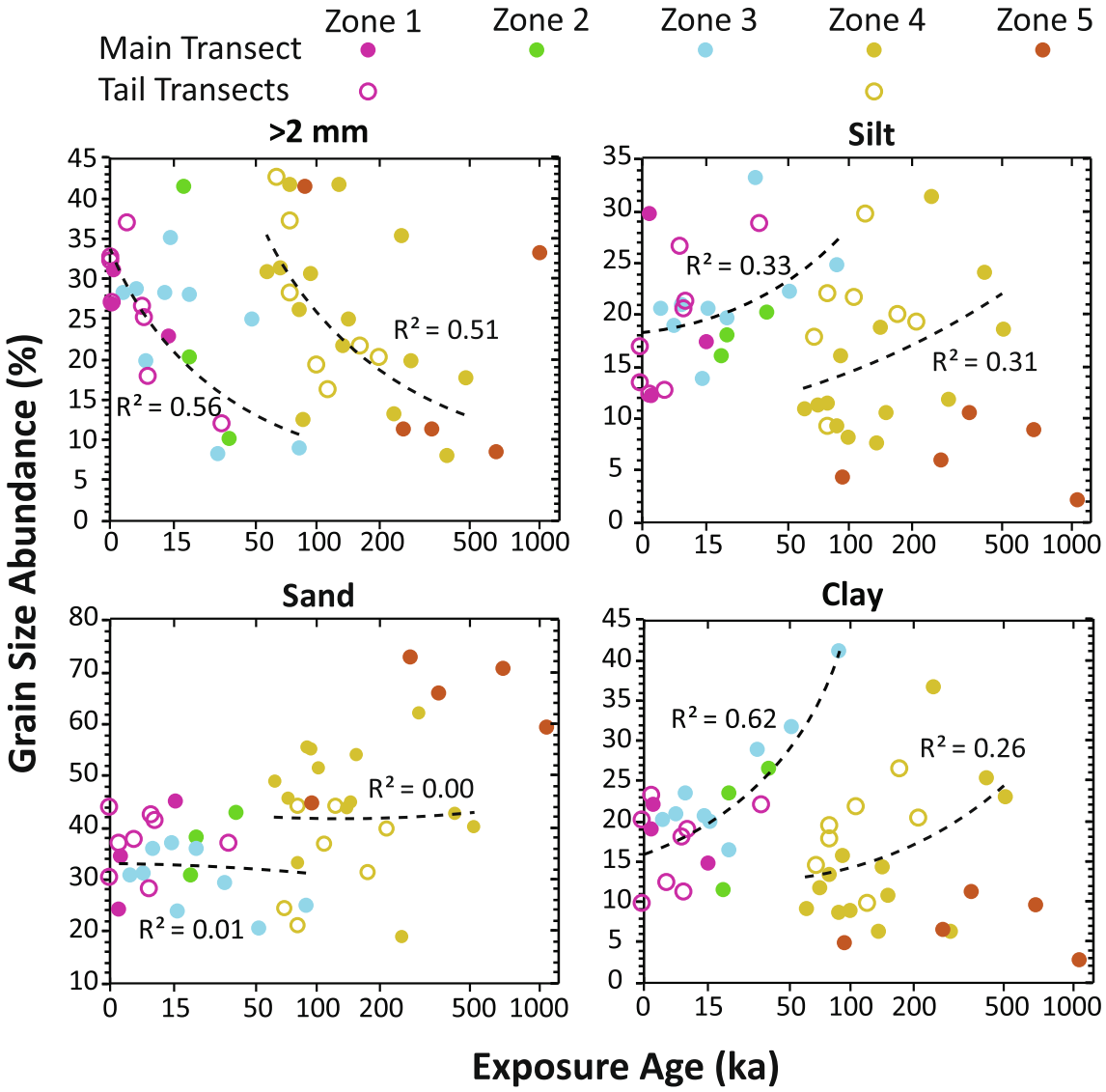

Fig. 3. Grain size distribution with boron proxy exposure age in Mt. Achernar Moraine samples, with each of the geomorphic zones of the moraine (Fig. 1) labeled separately. Solid circles depict samples from the main transect; open circles depict samples from the tail transects. Trends are plotted separately for Zones 1–3 and Zone 4. No trend is depicted for Zone 5. Error in the boron-based exposure age is within symbol size (Appendix B).

minerals such as carbonates, 0.5 M hydrochloric acid (HCl) – soluble minerals such as amorphous oxyhydroxides, and 1 M hydroxylamine hydrochloride (NH_2OH-HCl) - soluble minerals such as crystalline oxides (e.g. Wiederhold et al., 2007). All extracts were measured for major elements on a Perkin-Elmer Optima 7000 inductively coupled plasma – optical emission spectrometer (ICP-OES). In 47 of 58 samples, the bulk elemental composition of the <63 μm fraction was analyzed for major and trace elemental composition by fusion, total dissolution, and inductively coupled plasma mass spectrometry at Act Labs. In 45 of 58 samples, mineral abundance in the <63 μm fraction was measured through powder X-ray diffraction and Rietveld refinement. On these samples, clay speciation was also assessed by X-ray diffraction analysis of the <1 μm fraction, isolated by settling in water. The methods for sequential extraction and X-ray diffraction are identical to those described in greater detail in Graly et al. (2020).

We employed a salt accumulation proxy for exposure age to assess change in sediment composition as a function of surface exposure age. Though there is a general relationship between distance from the active ice margin and moraine surface exposure age, the complex history of ice flow into the moraine has created regions where an age-distance relationship does not apply (Graly et al., 2018b; Kaplan et al., 2017). At sites where both were measured, soil boron content corresponds quite closely ($R^2 > 0.99$) with exposure age assessed through cosmogenic isotopes (Graly et al., 2018b), and we treat it as an accurate measure of relative age throughout the moraine. We thus assign an

Please cite this article in press as: Graly J. A., et al. Chemical weathering signatures at Mt. Achernar, Central Transantarctic Mountains II: Surface exposed sediments. *Geochim. Cosmochim. Acta* (2022), https://doi.org/10.1016/j.gca.2022.06.024

age to every sample collected in the moraine, not only to those with a corresponding cosmogenic isotope age. The ages are calculated from a B-Age slope described by the linear formula: Age (ka) = 160.7 ± 4.6·[B] (μmol per g) – 13.7 ± 6.2. This slope derives from 11 locations where a surface sediment boron concentration was measured adjacent to a boulder analyzed for cosmogenic isotopes. For most samples, error in the boron measurements is trivial compared with the uncertainty in this correlation.

2.3. Data Analysis

In the analysis of the geochemical data from Mt. Achernar Moraine, we describe the significance and magnitude of the changes in the moraine surface with time, separating the signal of surface alteration processes from changes in the underlying material provided from the subglacial environment. We then develop a series of equations to describe the relative contribution of physical deterioration, chemical weathering, and atmospheric deposition to the observed mineral and chemical composition of the <63 μm fraction. We lastly use the limited data we have regarding distribution of the chemical weathering products with depth to infer chemical weathering and CO_2 drawdown rates.

Grain size, bulk chemistry, and mineralogy of moraine surface sediments are assumed to be controlled primarily by the length of surface exposure and by the composition of material provided from the subglacial environment. To separate these signals, we employ multi-variate linear regression to predict each of these parameters as a function of boron-proxy exposure age and 40–100 mm rock clast composition. And while we do not expect the clast composition to represent the material input to the <63 μm fraction in the subglacial environment on a one-to-one basis (Graly et al., 2020), we expect variation in clast composition to reflect variation in the source material, variation in the subglacial processes causing comminution of the underlying rock, or some combination of both. Because the compositional differences between the igneous clasts and the sedimentary / metasedimentary clasts are far larger than any differences within the two groups (Graly et al., 2020), clast composition was reduced to a single factor representing the percentage of clasts of igneous rock composition. At the Mt. Achernar site, the igneous rocks are almost entirely clasts of the Ferrar Dolerite (Bader et al., 2017). For the 21 main transect samples where a 40–100 mm clast sample was collected together with a sediment sample, we assessed the correlation between bulk composition and the percentage of clasts of igneous composition. We then used the multiple regression trend between percent igneous composition and each of the major elements to estimate a percentage igneous composition for the remaining 26 samples where bulk elemental composition was assessed but a clast sample was not collected. We then performed a multi-variate regression for each element, mineral, and grain size fraction in terms of both exposure age and percent igneous rock. Statistical significance of the regressed trends was tested against a zero-slope null hypothesis. For some variables, trends were also assessed independently for different sections of the moraine. Unless otherwise noted, trends are treated as statistically significant if $p \leq 0.05$. For analysis, we normalized these data either for variation by clast composition (Figs. 4–6) or for variation by exposure age (Figs. 7–9). In the clast composition normalization, the clast composition trend is used to adjust the data to values found at 50% igneous rock; in the exposure age normalization, the exposure age trend is used to adjust the data to the values of freshly emerging sediment (i.e. exposure age = 0).

With the mineralogy of the rocks supplied from subglacial environment known (Graly et al., 2020), we can describe the inputs that cause change in element abundance on the moraine surface. The underlying reason for change in the abundance of any element or mineral in the <63 μm fraction is the addition of new material (or, potentially, removal of existing material). The change in fractional abundance of any material component (elements, minerals, etc.) depends on its initial abundance in the <63 μm fraction relative to its abundance in any newly added or removed material. If the material flux rate is constant with time, the fractional abundance as a function of time (t) is described:

$$X = \frac{X_i + tF_X}{1 + t\sum_{j=1}^{n} F_j} \quad (1)$$

where X_i is the initial abundance of component X in the <63 μm fraction, F_X is the flux of component X into the <63 μm fraction, and F_j refers to each of the n total components of flux into the <63 μm fraction.

For each major mineral in the underlying subglacial material, we numerically determined the best flux values (i.e. F_j) to match the changes in elemental abundance as a function of exposure age across the main transect of the moraine that we derived from linear regression. This was implemented in MATLAB using the fmincon function (Code in Appendix A). This approach fits a non-linear equation to linear trend derived from regression. However, for the values employed, Eq. (1) closely approaches linearity. The mineral fluxes into the <63 μm fraction were calculated through an error minimization for all major elements:

$$E = \frac{E_i + t\sum_{j=1}^{n} E_j F_j}{1 + t\sum_{j=1}^{n} F_j} \quad (2)$$

where E is the element's abundance at time t, E_i is the measured initial abundance of the element in the <63 μm fraction of freshly emerging sediments with minimal salt development, E_j is the abundance in wt. fraction of element E in each of n minerals , and F_j is the flux of those minerals into the <63 μm fraction. For solid solution minerals (pyroxenes, feldspars) E_j values derive from Rietveld refinement of the X-ray diffraction data (Graly et al., 2020). F_j terms were included for every mineral with >1% abundance in the underlying rock. The amorphous components of sedimentary rock at the site were included to represent intergranular cements that can be a detrital component added to the <63 μm fraction as rocks break down under physical weathering.

We also included flux terms for atmospheric input. The relative input of sulfate, nitrate, and chloride was determined from the regression of their abundance in the

Please cite this article in press as: Graly J. A., et al. Chemical weathering signatures at Mt. Achernar, Central Transantarctic Mountains II: Surface exposed sediments. *Geochim. Cosmochim. Acta* (2022), https://doi.org/10.1016/j.gca.2022.06.024

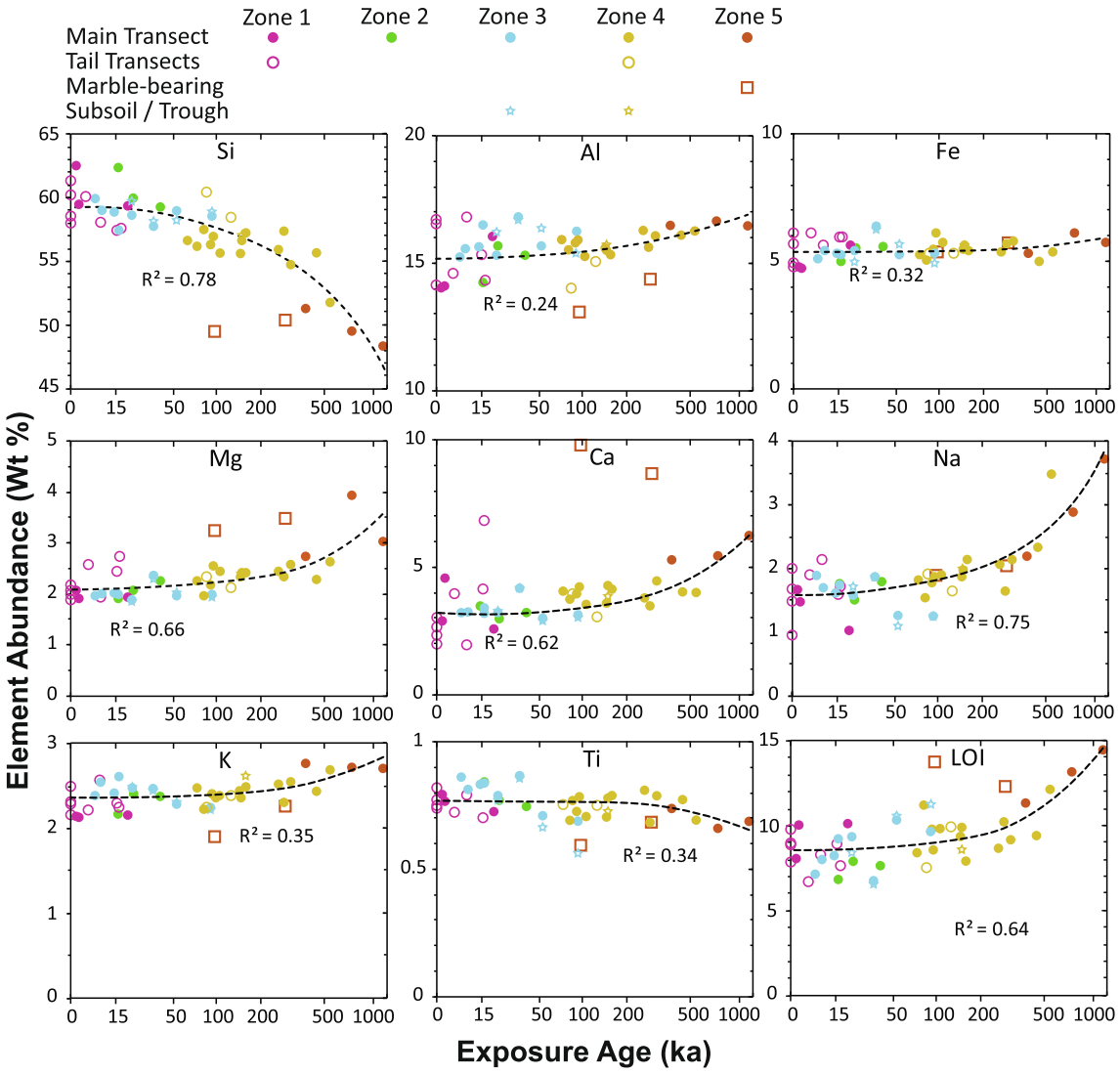

Fig. 4. Major elements and LOI in the <63 μm fraction as a function of exposure age (boron proxy). All data have been normalized for changes as a function of Ferrar Dolerite abundance in the pebble and cobble fraction. R^2 values are calculated from main transect samples, with tail transect samples, two samples from a zone bearing limestone and marble pebbles (5A & 5B), and samples from the soil subsurface or moraine troughs (n = 5) plotted separated. The trough and subsoil samples are plotted at the age of a corresponding surface sample. Colors reflect geomorphic zones per Fig. 1.

water-extracted fraction. Atmosphere-derived carbonate was inferred from the abundance of Ca and Mg in the acetic acid extraction, in which carbonate minerals dissolve. All these species are included in the loss on ignition (LOI) term. The salt- and carbonate-associated cations (Na, Ca, Mg, K) can enter these fractions either as atmosphere-derived salt, or as products chemically leached by atmospheric acids (carbonic, nitric, sulfuric, etc.). We therefore need to know the ratio of acid deposition to salt deposition at the Mt. Achernar Moraine site. The original atmospheric acids are preserved in ice and have been well described in ice cores (Legrand and Mayewski, 1997). This record is especially detailed at Vostok (Legrand et al., 1988), but similar records exist at Dominion Range (100 km from our site) (Mayewski et al., 1995; Mayewski et al., 1990) and in a number of other interior Antarctic locations (e.g. Watanabe et al., 2003; Wolff et al., 2010). We use the Pleistocene Vostok data to model salt fallout at our site, as the Dominion Range data primarily cover the Holocene and are incomplete in the Pleistocene section of the core (e.g. nitrate was not measured). We also included terms for the leaching of Ca, Na, and Mg from the coarser size fractions in assessing the evolution of the <63 μm fraction's composition (i.e. for the case when the weathering products apart from mobile cations remain in the coarser grain size fractions).

Once the mineral flux into the <63 μm fraction from rock or atmospheric sources is known, we can compare the difference between these fluxes and our mineralogical observations to assess chemical alteration within the <63 μm fraction. For each mineral, mineralogical changes within the <63 μm fraction (M_{leach}) were assessed from

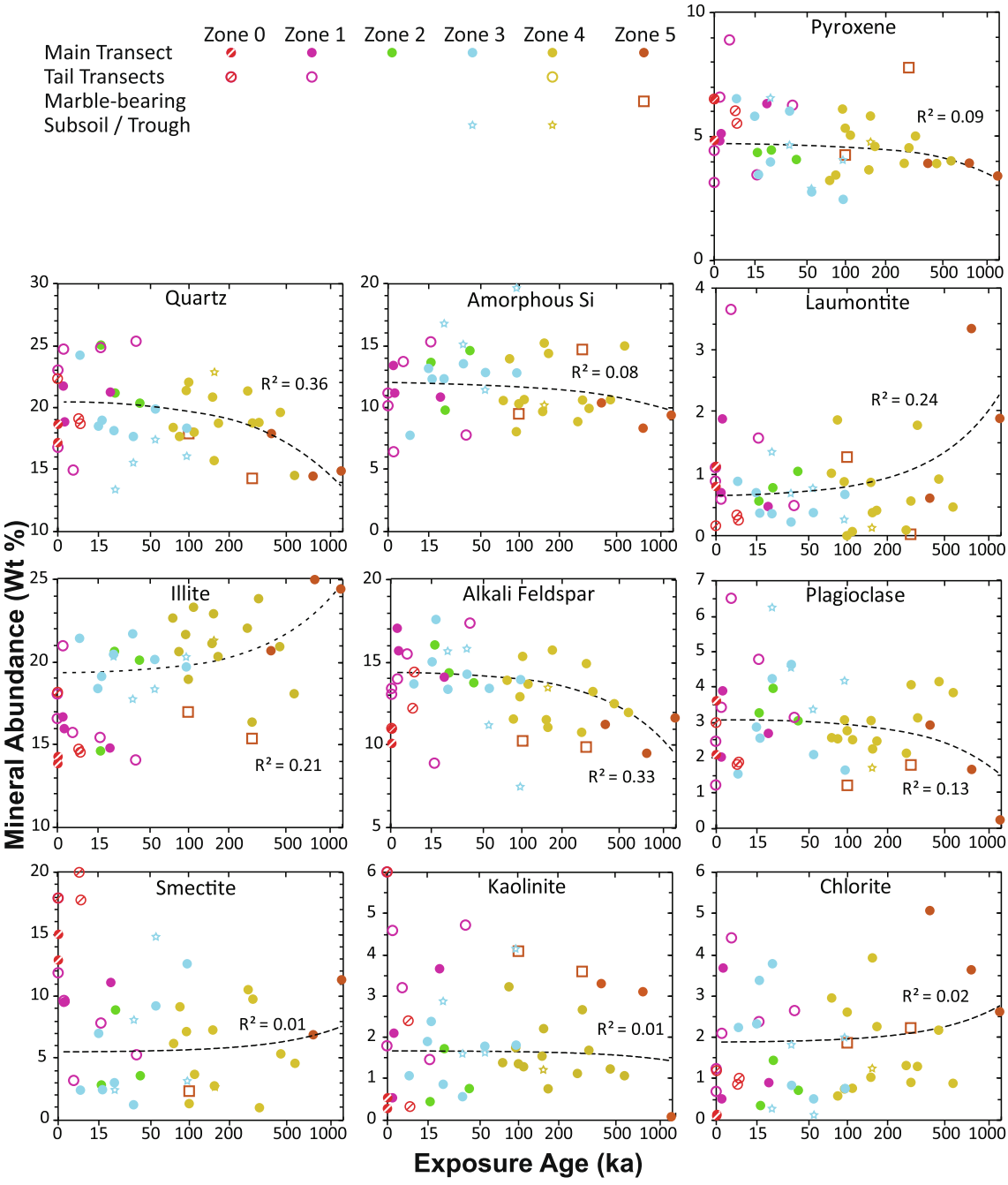

Fig. 5. Mineral abundances from quantitative X-ray diffraction of the <63 μm fraction as a function of exposure time (boron proxy). All data have been normalized for changes as a function of Ferrar Dolerite abundance in the pebble and cobble fraction. Samples for which bulk elemental abundance was not measured cannot be normalized for cobble abundance and are marked with a slash symbol. The data classification otherwise follows Fig. 4.

the linear trend in mineral abundance from X-ray diffraction as a function of exposure time, with the physical flux (F_M) calculated by Eq. (2):

$$M = \frac{M_i + t(F_M - M_{leach})}{1 + t\sum_{j=1}^{n} F_j} \quad (3)$$

where M is the mineral abundance at time t, and M_i is the mineral abundance in freshly emerging sediments. M_{leach} can be positive if the mineral is precipitated from the weathering of other minerals (i.e. for clays). Theoretically, the M_{leach} value for amorphous content and leached salts is the inverse of the sum of the other M_{leach} values.

To assess total chemical fluxes from the atmosphere to the moraine sediment and total chemical weathering within the moraine, we need to estimate the total content of chemical weathering products within the sediment column.

Please cite this article in press as: Graly J. A., et al. Chemical weathering signatures at Mt. Achernar, Central Transantarctic Mountains II: Surface exposed sediments. *Geochim. Cosmochim. Acta* (2022), https://doi.org/10.1016/j.gca.2022.06.024

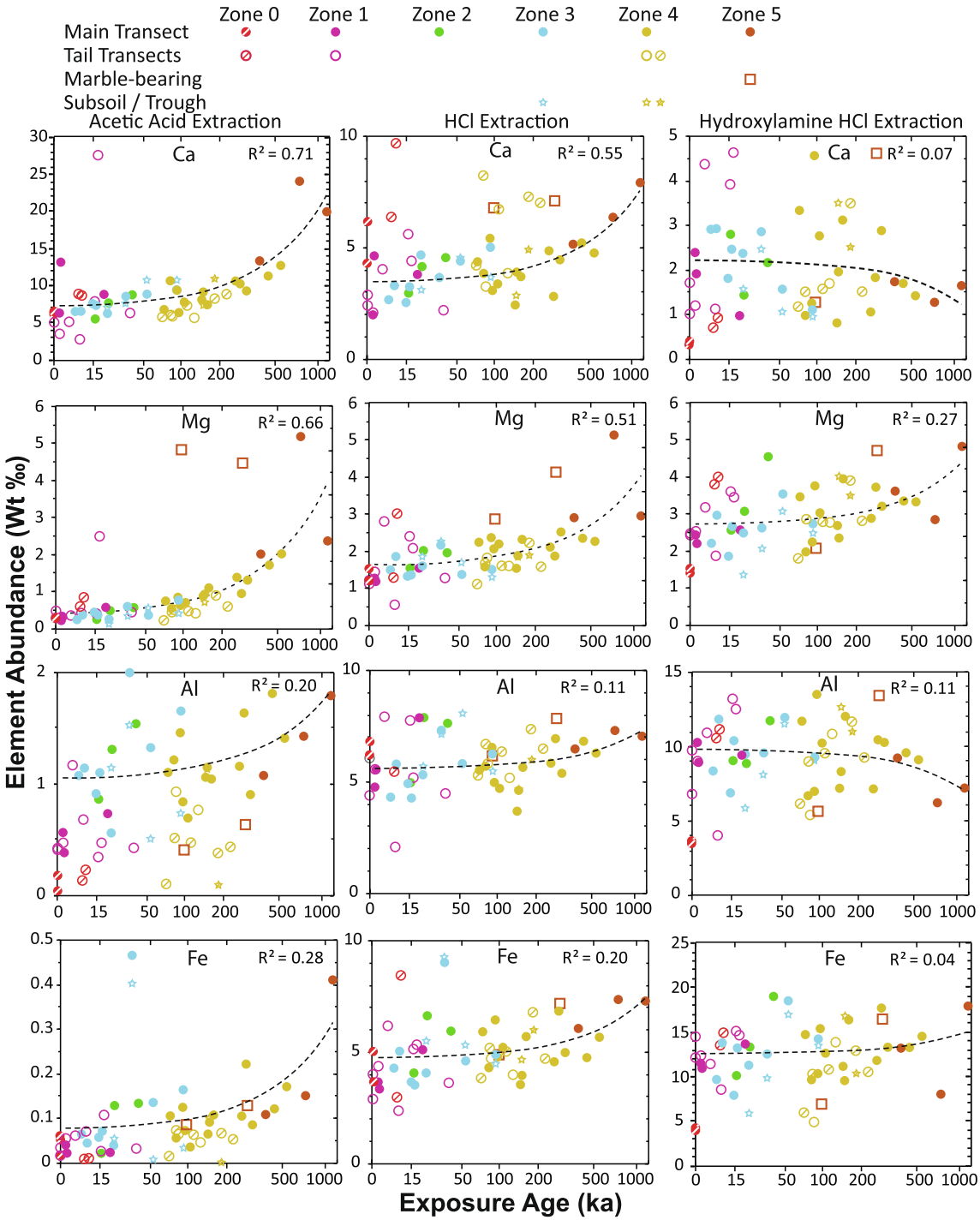

Fig. 6. Elemental abundances from the sequential acetic acid, HCl, and hydroxylamine hydrochloride extractions of the <63 μm fraction as a function of exposure age (boron proxy). All data have been normalized to changes as a function of Ferrar Dolerite abundance in the pebble and cobble fraction. The data classification follows Fig. 5.

Because, in most cases, we have only analyzed the <63 μm fraction of a single sample collected near the top of the sediment column, the total weathering product content of the moraine can only be estimated to first approximation. The total deposited mass will follow the general formula for any mineral, element, or compound X:

$$\frac{dm}{dt} = \rho \frac{dX}{dt} \frac{dH}{dt} \frac{dC}{dt} \quad (4)$$

where m is the total mass per square area of X vertically integrated through the sediment column of the moraine, ρ is average density of the moraine sediment, X is the fractional mass of the component in the surface sample, H is

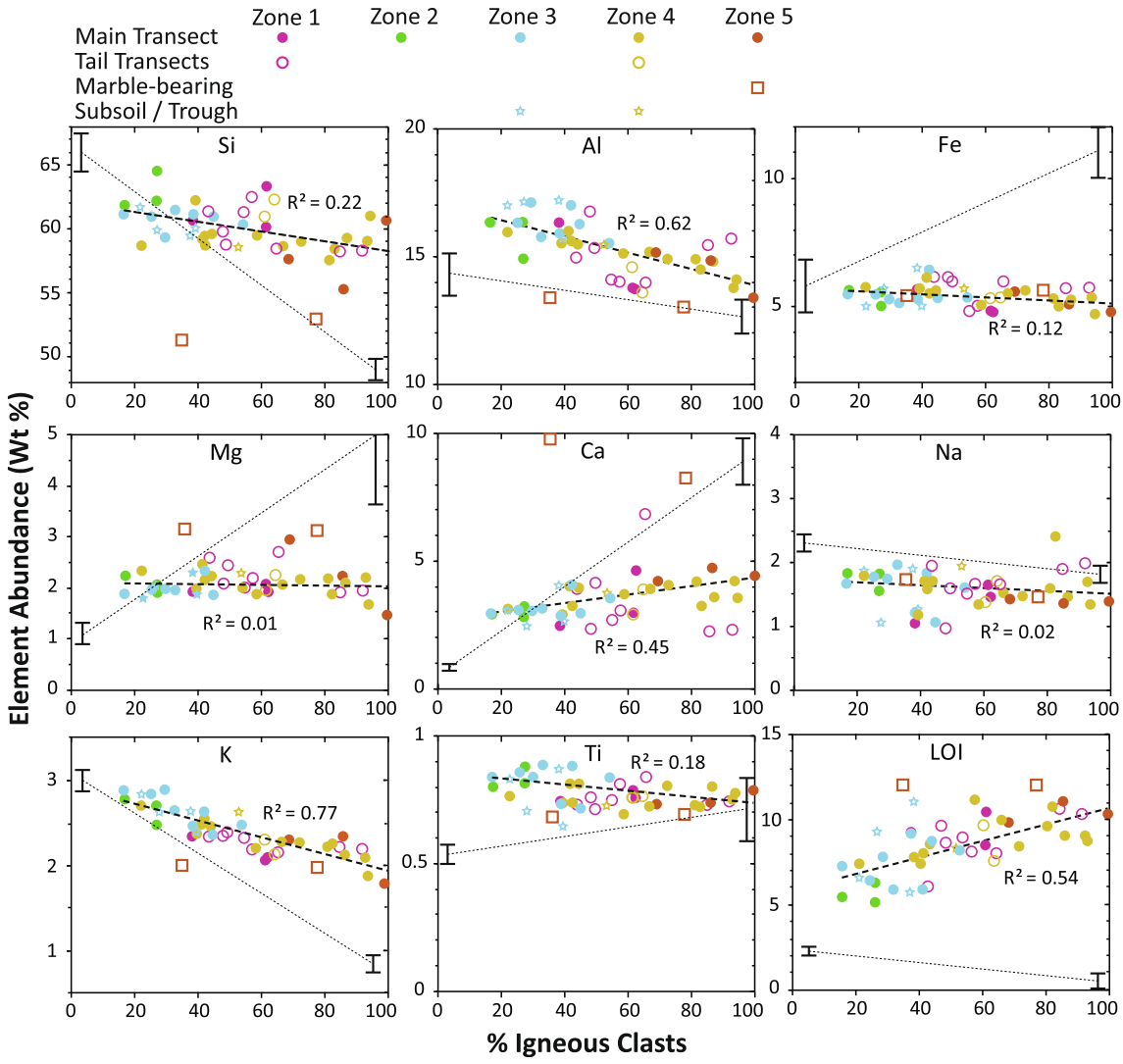

Fig. 7. Major elements and LOI data in the <63 μm fraction as a function of the relative proportion of Ferrar Dolerite in the pebble and cobble clasts on the moraine surface. All data have been normalized for changes as a function of exposure age (boron proxy). The barred ranges reflect the composition of sedimentary rock (at 0%) and igneous rock (at 100%) per Graly et al. (2020). The dashed line is a putative mixing line between them. Data classification otherwise follows Fig. 4.

the thickness of the moraine, and C is a constant relating the average mass at depth to that of the near surface measurement.

To estimate solutions for Eq. (4), we use the derivative of Eq. (1) for $\frac{dX}{dt}$ and estimate $\frac{dH}{dt}$ and $\frac{dC}{dt}$ from empirical observations of changes in the moraine with exposure age. In many samples the thickness of the moraine was directly observed by excavating to the ice below. Where the moraine became too thick to attempt this (in Zone 4), a rod was inserted to depth. These are minimum depths, as we cannot confirm whether the rod stopped at ice or at a large cobble. Values for C were estimated for both salt species and carbonates. In this study, there are only two soils from the main transect in which an additional sample was taken below the soil oxidation horizon. However, salt and carbon concentration measurements from nine soil profiles (2–4 samples per profile) were also reported from Mt. Achernar Moraine by Scarrow et al. (2014). In these 11 soil profiles, we estimate the total abundance of salt and carbonate minerals and correlate these to their surface concentrations. As salt and carbonate minerals are the principal repositories for chemically leached cations, we are able to estimate total atmospheric flux and chemical alteration across the time transect of the moraine.

3. RESULTS

3.1. Grain Size

Clast composition has no statistically significant effect on sediment grain size distribution (Table 1). We therefore consider grain size variation only as a function of exposure age. Across the entire data set, we see a weak but statistically significant ($R^2 = 0.16$) decline in >2 mm particle abun-

Please cite this article in press as: Graly J. A., et al. Chemical weathering signatures at Mt. Achernar, Central Transantarctic Mountains II: Surface exposed sediments. *Geochim. Cosmochim. Acta* (2022), https://doi.org/10.1016/j.gca.2022.06.024

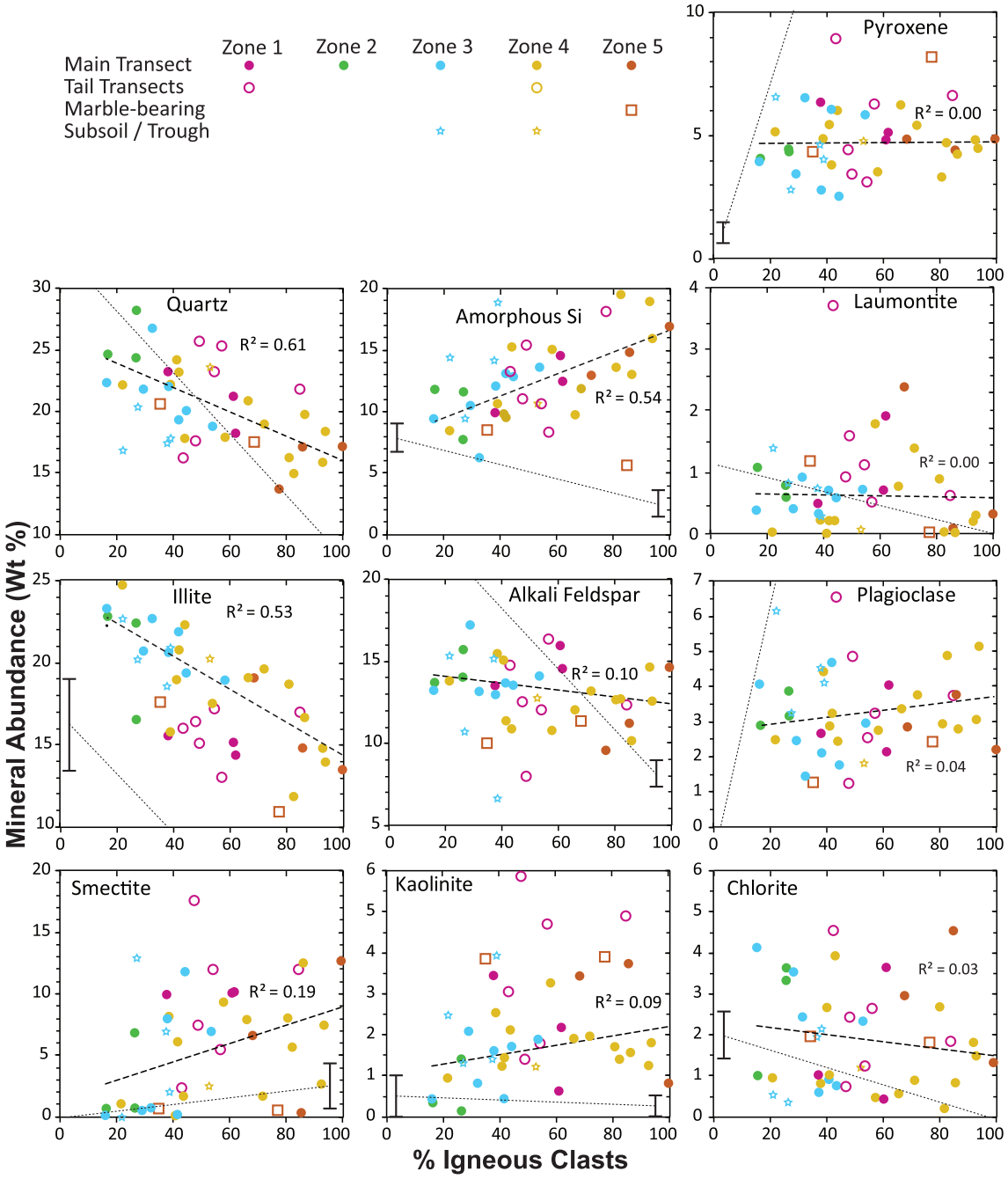

Fig. 8. Mineral abundances from quantitative X-ray diffraction in the <63 μm fraction as a function of the relative proportion of Ferrar Dolerite in the pebble and cobble clasts on the moraine surface. All data have been normalized for changes as a function of exposure age (boron proxy). The barred ranges and data classification follow Fig. 7. Minerals which are absent from igneous or sedimentary rocks per Graly et al. (2020) show no barred range and intersect the x-axis at zero. In some cases (e.g. quartz), the igneous and/or sedimentary rock endmembers are off the range of the plot.

dance with exposure age (Table 1). However, there are substantially stronger trends when the principal geomorphic zones of the moraine are examined independently (Fig. 3). Zones 1–3 and the lateral moraine portions of the tail transects show declining abundance of >2 mm particles and rising silt and clay content with age. The same pattern occurs separately in Zone 4, but with the coarse particle abundance at the beginning of Zone 4 being far higher than at the back end of Zone 3. The same stepwise change from finer to coarse sediments occurs between Zone 2 and Zone 3. Sand content does not significantly change across Zones 1–3 or across Zone 4, though Zone 4 is higher step-wise. The youngest 4 samples in Zone 5 plot along a similar trend to Zone 4 for coarse (>2 mm) sediment, but with higher sand and lower silt and clay. The oldest Zone 5 sample is coarser still.

Please cite this article in press as: Graly J. A., et al. Chemical weathering signatures at Mt. Achernar, Central Transantarctic Mountains II: Surface exposed sediments. *Geochim. Cosmochim. Acta* (2022), https://doi.org/10.1016/j.gca.2022.06.024

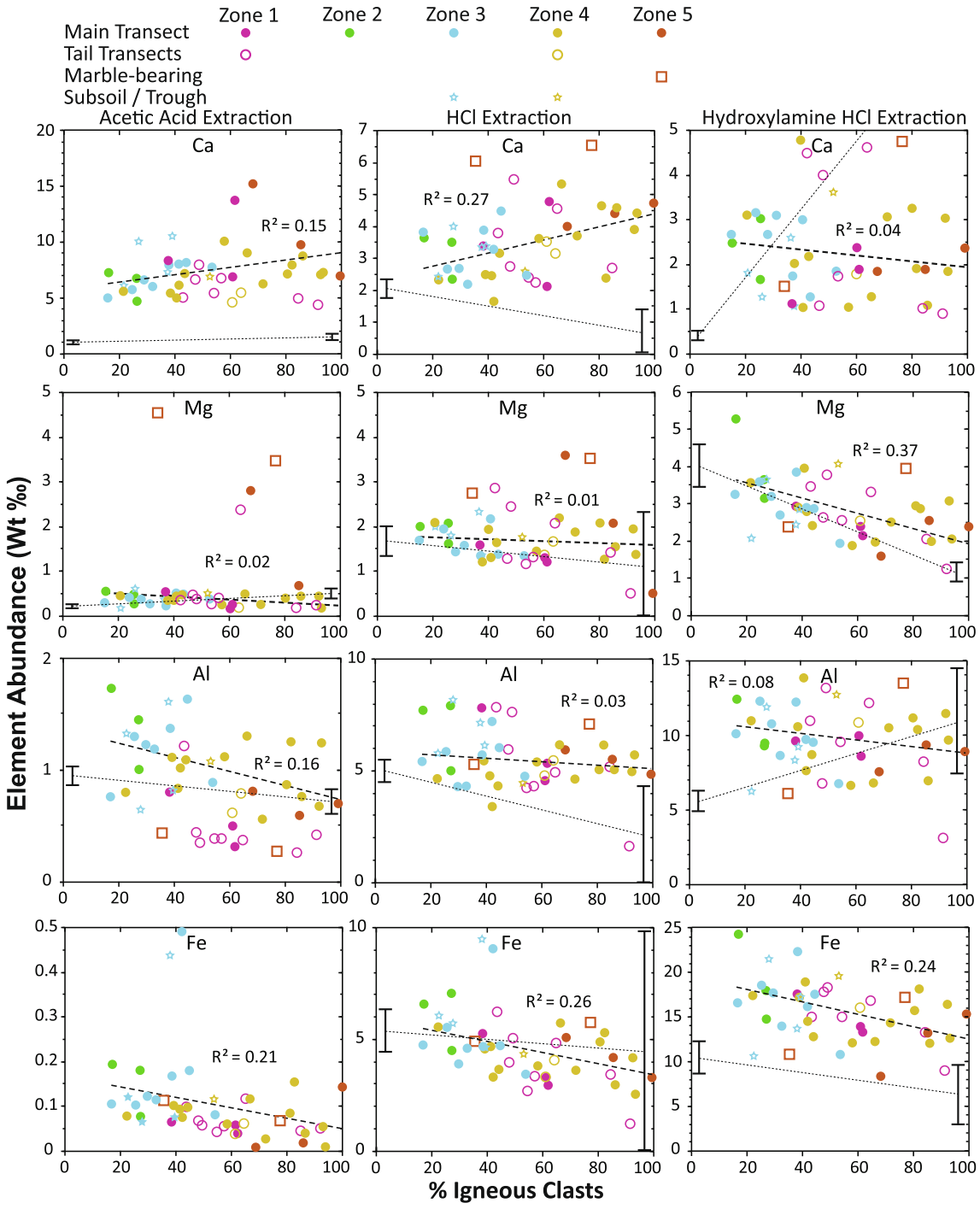

Fig. 9. Elemental abundances from the sequential acetic acid, HCl, and hydroxylamine hydrochloride extractions of the <63 μm fraction as a function of the relative proportion of Ferrar Dolerite in the pebble and cobble clasts on the moraine surface. All data have been normalized for changes as a function of exposure age (boron proxy). The barred ranges and data classification follow Fig. 7.

3.2. Age Control on Bulk Elemental Composition and Mineralogy

When normalized for clast composition, all major elements in the <63 μm fraction show statistically significant change as a function of exposure age (Fig. 4). Si and Ti abundances decrease with exposure time whereas Al, Fe, Ca, Mg, Na, K and LOI increase with exposure time. Over a 1 Ma interval, these changes represent a 12.0 ± 1. 6 wt% decrease in Si countered by a 5.8 ± 1.1 wt% increase in LOI, a 1.9 ± 0.3 wt% increase in Na, a 1.9 ± 0.4 wt% increase in Ca, and a 1.4 ± 0.3 wt% increase in Mg, along with smaller changes in other elements (Fig. 4, Table 1). A few of the minor, trace, and rare earth

Please cite this article in press as: Graly J. A., et al. Chemical weathering signatures at Mt. Achernar, Central Transantarctic Mountains II: Surface exposed sediments. *Geochim. Cosmochim. Acta* (2022), https://doi.org/10.1016/j.gca.2022.06.024

Table 1
Regression trends (underlying data is in Appendix B).

Factor	Initial value (wt.%)	Age Trend (Δ/Ma)	Age p-value	Composition Trend (Δ)	Composition p-value	R^2 (total)
A. Grain Size						
Cobbles All	30.2 ± 4.2	−30.3 ± 14.6	**0.045**	−5.1 ± 8.2	0.537	**0.16**
Cobbles Zone 1–3	28.9 ± 4	−204 ± 51.5	**0.001**	5.8 ± 8	0.473	**0.43**
Cobbles Zone 4–5	44.2 ± 8.1	−64.6 ± 25.1	**0.028**	−17.7 ± 14	0.234	**0.57**
Sand All	37.5 ± 4.2	29.4 ± 18	0.112	−2.7 ± 8.3	0.748	0.08
Sand Zone 1–3	35.5 ± 3.5	6.8 ± 45.4	0.883	−2.4 ± 7	0.741	0.01
Sand Zone 4–5	53.1 ± 11	−17.2 ± 34	0.624	−8.1 ± 18.9	0.677	0.07
Silt All	15.6 ± 3	12 ± 12.9	0.361	3.2 ± 6	0.593	0.05
Silt Zone 1–3	15.4 ± 2.7	117.4 ± 35.5	**0.003**	2.2 ± 5.5	0.699	**0.36**
Silt Zone 4–5	4.9 ± 5.6	38.6 ± 17.4	**0.051**	7.1 ± 9.7	0.479	**0.45**
Clay All	16.8 ± 3.7	17.5 ± 16	0.280	0.7 ± 7.3	0.920	0.04
Clay Zone 1–3	16.8 ± 0.6	191.2 ± 48.4	**0.001**	−1.6 ± 5.8	0.789	**0.44**
Clay Zone 4–5	−2.1 ± 0	45.8 ± 22.9	**0.071**	17.1 ± 12.7	0.203	**0.45**
B. Major Elements						
Si	61.8 ± 0.8	−12 ± 1.6	**<0.001**	−3.4 ± 1.6	**0.044**	**0.84**
Al	17 ± 0.3	1.3 ± 0.6	**0.032**	−3.1 ± 0.6	**<0.001**	**0.51**
Fe	5.7 ± 0.2	0.9 ± 0.3	**0.01**	−0.7 ± 0.3	**0.03**	**0.23**
Mg	2.1 ± 0.1	1.4 ± 0.3	**<0.001**	−0.1 ± 0.3	0.671	**0.64**
Ca	2.7 ± 0.2	1.9 ± 0.4	**<0.001**	1.6 ± 0.5	**0.001**	**0.76**
Na	1.7 ± 0.1	1.9 ± 0.3	**<0.001**	−0.2 ± 0.3	0.536	**0.73**
K	2.9 ± 0.1	0.4 ± 0.1	**0.006**	−1 ± 0.1	**<0.001**	**0.68**
Ti	0.8 ± 0	−0.1 ± 0	**0.008**	−0.1 ± 0	**0.07**	**0.54**
LOI	5.9 ± 0.5	5.8 ± 1.1	**<0.001**	4.8 ± 1.1	**<0.001**	**0.83**
C. Minor Elements						
Mn	86.3 ± 1.9	−14 ± 3.9	**0.001**	15 ± 3.9	**0.001**	**0.38**
P	153.4 ± 6.5	0 ± 0	0.215	−29.5 ± 13.5	**0.038**	**0.34**
Sc	17.4 ± 0.4	0.5 ± 0.9	0.604	−0.1 ± 0.9	0.899	0.01
V	109.9 ± 3.7	−2.9 ± 7.7	0.710	−2.1 ± 7.8	0.790	0.02
Ba	799.6 ± 24.6	0.9 ± 50.7	0.986	−260 ± 51.2	**<0.001**	**0.62**
Sr	268.5 ± 21.1	281.5 ± 43.5	**<0.001**	−95 ± 43.9	**0.04**	**0.64**
Y	32.3 ± 1.2	−1.7 ± 2.4	0.484	−7.8 ± 2.4	**0.004**	**0.46**
Zr	260.5 ± 25.7	−160.2 ± 53	**0.005**	128.7 ± 53.5	**0.023**	**0.26**
Cr	86.9 ± 4.3	14.5 ± 9	0.116	−30.9 ± 9.1	**0.002**	**0.31**
Co	16.5 ± 0.6	4.4 ± 1.3	**0.002**	−2.2 ± 1.3	0.112	**0.31**
Ni	38.2 ± 3.6	10.1 ± 7.4	0.183	−10.6 ± 7.4	0.164	0.08
Cu	44.2 ± 10.5	78.6 ± 21.8	**0.001**	−30.8 ± 22	0.172	**0.35**
Zn	89.8 ± 5.8	60.5 ± 12	**<0.001**	−47.9 ± 12.1	**<0.001**	**0.49**
Ga	21 ± 0.7	2.2 ± 1.4	0.136	−5 ± 1.4	**0.002**	**0.33**
Ge	1.7 ± 0.2	1.8 ± 0.4	**<0.001**	−0.5 ± 0.4	0.275	**0.43**
Rb	106.2 ± 2.4	18.1 ± 5	**0.001**	−31.5 ± 5.1	**<0.001**	**0.59**
Nb	10.9 ± 0.5	−1.6 ± 1	0.135	−0.9 ± 1	0.403	**0.23**
Ag	1 ± 0.2	−0.7 ± 0.5	0.185	0.8 ± 0.5	0.123	0.09
Sn	3.4 ± 0.4	0.6 ± 0.9	0.523	−1.2 ± 0.9	0.201	0.06
Cs	5.6 ± 0.3	2.2 ± 0.5	**<0.001**	−1 ± 0.6	**0.071**	**0.38**
La	46.5 ± 2.2	1.2 ± 4.6	0.801	−15.3 ± 4.6	**0.003**	**0.38**
Ce	93.3 ± 4.1	1.2 ± 8.4	0.891	−30.3 ± 8.5	**0.001**	**0.43**
Pr	10.3 ± 0.4	−0.3 ± 0.9	0.760	−2.8 ± 0.9	**0.005**	**0.40**
Nd	38.9 ± 1.4	−2.1 ± 3.4	0.535	−8.9 ± 3.4	**0.014**	**0.37**
Sm	7.4 ± 0.3	−0.7 ± 0.6	0.236	−1.6 ± 0.6	**0.016**	**0.43**
Eu	1.6 ± 0	−0.1 ± 0.1	0.243	−0.4 ± 0.1	**<0.001**	**0.63**
Gd	6.2 ± 0.2	−0.8 ± 0.5	0.116	−1 ± 0.5	**0.043**	**0.42**
Tb	1.0 ± 0	−0.1 ± 0.1	**0.031**	−0.2 ± 0.1	**0.01**	**0.57**
Dy	5.6 ± 0.2	−0.6 ± 0.4	0.167	−1 ± 0.4	**0.024**	**0.43**
Ho	1.1 ± 0	−0.1 ± 0.1	**0.093**	−0.1 ± 0.1	**0.054**	**0.42**
Er	3.2 ± 0.1	−0.4 ± 0.2	**0.041**	−0.4 ± 0.2	**0.055**	**0.47**
Tm	0.5 ± 0	−0.1 ± 0	**0.044**	−0.1 ± 0	**0.049**	**0.47**
Yb	3.2 ± 0.1	−0.5 ± 0.2	**0.022**	−0.3 ± 0.2	0.163	**0.44**
Lu	0.5 ± 0	−0.1 ± 0	**0.012**	0 ± 0	0.559	**0.38**
Hf	7.1 ± 0.5	−3.6 ± 1.1	**0.002**	2.3 ± 1.1	**0.045**	**0.29**
Ta	0.9 ± 0	0 ± 0.1	0.983	−0.3 ± 0.1	**0.002**	**0.42**

Please cite this article in press as: Graly J. A., et al. Chemical weathering signatures at Mt. Achernar, Central Transantarctic Mountains II: Surface exposed sediments. *Geochim. Cosmochim. Acta* (2022), https://doi.org/10.1016/j.gca.2022.06.024

Tl	0.6 ± 0	−0.2 ± 0.1	**0.009**	0 ± 0.1	0.8	**0.36**
Pb	24.2 ± 1.4	3.2 ± 2.9	0.275	−11.5 ± 2.9	**0.001**	**0.41**
Th	14.8 ± 0.5	−0.5 ± 1.1	0.674	−2.4 ± 1.1	**0.038**	**0.28**
U	3.6 ± 0.1	0 ± 0.2	0.950	−0.7 ± 0.2	**0.007**	**0.34**
D. Minerals						
Quartz	26.1 ± 1	−8.1 ± 2.1	**0.001**	−9.7 ± 2.1	**<0.001**	**0.79**
Pyroxene	4.7 ± 0.5	−1.3 ± 1	0.228	0.1 ± 1.1	0.939	0.08
Alkali Feldspar	14.6 ± 0.8	−4.4 ± 1.6	**0.01**	−2.1 ± 1.6	0.208	**0.47**
Plagioclase Feldspar	2.7 ± 0.5	−1.4 ± 0.9	0.134	0.8 ± 0.9	0.42	0.09
Illite	24.6 ± 1.2	4.9 ± 2.4	**0.053**	−10.4 ± 2.5	**<0.001**	**0.42**
Smectite	1.5 ± 1.9	1.9 ± 3.8	0.631	7.4 ± 3.9	**0.069**	**0.24**
Kaolinite	1 ± 0.5	−0.3 ± 0.9	0.776	1.2 ± 1	0.223	0.07
Chlorite	2.3 ± 0.7	0.8 ± 1.3	0.538	−0.9 ± 1.3	0.521	0.02
Laumontite	0.6 ± 0.3	1.4 ± 0.6	**0.033**	−0.1 ± 0.6	0.935	**0.24**
Amorphous Si	7.5 ± 1	−2.4 ± 2.1	0.265	9.2 ± 2.1	**<0.001**	**0.44**
Uncoordinated LOI	3 ± 0.5	−0.9 ± 0.9	0.351	3 ± 0.5	**<0.001**	**0.24**
E. Sequential Extractions						
Na H2O	0.1 ± 0	1.6 ± 0.1	**<0.001**	−0.1 ± 0.1	0.345	**0.86**
K H2O	0 ± 0	0 ± 0	**<0.001**	0 ± 0	0.102	**0.46**
Ca H2O	0.1 ± 0.1	0.8 ± 0.3	**0.008**	0 ± 0.2	0.82	**0.33**
Mg H2O	0 ± 0	0.1 ± 0	**<0.001**	0 ± 0	0.287	**0.67**
Cl H2O	0 ± 0	0.6 ± 0.1	**<0.001**	0.1 ± 0	0.159	**0.81**
SO42 H2O	0.4 ± 0.2	4.0 ± 0.8	**<0.001**	−0.1 ± 0.4	0.833	**0.59**
Fl H2O	0 ± 0	0.04 ± 0.01	**<0.001**	0 ± 0	0.641	**0.59**
NO3 H2O	0.1 ± 0	1.1 ± 0.1	**<0.001**	−0.2 ± 0.1	0.047	**0.74**
Total Salts	0.6 ± 0.4	8.2 ± 1.3	**<0.001**	−0.3 ± 0.7	0.733	**0.68**
Na Acetic	0.03 ± 0.01	0.1 ± 0.02	**<0.001**	0 ± 0	0.223	**0.86**
K Acetic	0.02 ± 0.002	0.002 ± 0.003	0.496	−0.008 ± 0.003	**0.02**	**0.20**
Ca Acetic	0.6 ± 0.1	1.3 ± 0.2	**<0.001**	0.4 ± 0.2	0.088	**0.77**
Mg Acetic	0.1 ± 0	0.3 ± 0.1	**<0.001**	0 ± 0.1	0.532	**0.88**
Fe Acetic	0.01 ± 0.004	0.02 ± 0.01	**0.014**	0 ± 0	0.152	**0.20**
Al Acetic	0.1 ± 0	0.1 ± 0	**0.042**	−0.1 ± 0	0.073	**0.16**
P Acetic	0.01 ± 0.002	−0.005 ± 0.005	0.32	0 ± 0	0.634	0.09
Inferred CO3	1 ± 0.2	2.7 ± 0.4	**<0.001**	0.4 ± 0.4	0.268	**0.77**
Na HCl	0.01 ± 0	0.02 ± 0.004	**<0.001**	0 ± 0	0.365	**0.39**
K HCl	0.05 ± 0	0.02 ± 0.01	0.096	0 ± 0	0.047	**0.15**
Ca HCl	0.24 ± 0.04	0.4 ± 0.1	**<0.001**	0.2 ± 0.1	0.015	**0.70**
Mg HCl	0.17 ± 0.02	0.2 ± 0.05	**<0.001**	0 ± 0	0.666	**0.49**
Fe HCl	0.59 ± 0.06	0.2 ± 0.1	**0.045**	−0.2 ± 0.1	**0.04**	**0.18**
Al HCl	0.59 ± 0.05	0.2 ± 0.1	0.14	−0.1 ± 0.1	0.458	0.08
P HCl	0.01 ± 0	0 ± 0	0.622	0 ± 0	0.121	0.10
Mn HCl	0.01 ± 0	0 ± 0	0.927	0 ± 0	0.958	0.00
Inferred OOH	0.58 ± 0.06	0.4 ± 0.1	**0.001**	−0.2 ± 0.1	0.145	**0.35**
Na Hydrox	0.02 ± 0	0 ± 0	0.237	0 ± 0	0.058	0.13
K Hydrox	0.08 ± 0.01	0 ± 0	0.389	0 ± 0	0.054	0.13
Ca Hydrox	0.26 ± 0.04	−0.1 ± 0.1	0.271	−0.1 ± 0.1	0.409	0.15
Mg Hydrox	0.38 ± 0.03	0.1 ± 0.1	**0.015**	−0.2 ± 0.1	**0.003**	**0.30**
Fe Hydrox	1.91 ± 0.13	0.2 ± 0.3	0.411	−0.6 ± 0.3	**0.025**	**0.18**
Al Hydrox	1.08 ± 0.08	−0.2 ± 0.2	0.139	−0.2 ± 0.2	0.225	**0.25**
P Hydrox	0 ± 0	0 ± 0	0.684	0 ± 0	0.625	0.03
Mn Hydrox	0.01 ± 0	0 ± 0	0.685	0 ± 0	0.404	0.07

elements also show statistically significant trends with exposure age. Significant increases with sediment exposure age occur for Sr, Co, Cu, Zn, Ge, Rb, and Cs; significant decreases occur for Mn, Zr, Tb, rare earth elements Er–Lu, and Tl (Table 1).

Mineralogical changes in the <63 μm fraction as determined by powder X-ray diffraction show patterns that largely conform to what is observed in the major elements. In the composition normalized data, declines with exposure age in quartz and alkali feldspar abundance are statistically significant, as are increases in illite and laumontite (Fig. 5). Over the 1 Ma interval, these changes represent loss of 6.1 ± 2.1 wt% quartz and 4.4 ± 1.6 wt% alkali feldspar, countered by a gain of 4.9 ± 2.4 wt% illite and 1.4 ± 0.6 wt% laumontite (Table 1). Changes in other minerals are not statistically significant but could represent a slight loss in plagioclase and pyroxene and a slight gain in smectite and chlorite with time. In net, the abundance of crystalline minerals declines with exposure age, paralleling the gain in loss on ignition.

Please cite this article in press as: Graly J. A., et al. Chemical weathering signatures at Mt. Achernar, Central Transantarctic Mountains II: Surface exposed sediments. *Geochim. Cosmochim. Acta* (2022), https://doi.org/10.1016/j.gca.2022.06.024

The gain in LOI and X-ray amorphous substances with exposure age (Figs. 4, 5) is well documented in the sequential extractions, which show build-up of water soluble (Graly et al., 2018b), CH_3COOH-soluble and HCl-soluble elements (Fig. 6, Table 1). The NH_2OH-HCl extractions show relatively little change with exposure age (Fig. 6, Table 1). Because salt content (specifically boron) is used as the age proxy, there are unsurprising and strongly linear correlations between exposure age and water extracted species, representing a total gain in salt content of 8.2 ± 1.3 wt % over the 1 Ma interval (Table 1). In the CH_3COOH-extracted fraction, there are significant positive correlations between sediment surface exposure age and composition-normalized CH_3COOH-extractable Ca, Mg, Al, and Fe. If CH_3COOH-extractable Ca and Mg are interpreted as carbonate mineral dissolution, this represents a gain of 4.4 ± 0.6 wt% in calcite and dolomite (Table 1). Calcite and dolomite are often below detection limits in the XRD data (Appendix B), making this calculation more reliable, though some portion of the CH_3COOH-extractable Ca and Mg may derive from cation exchange on or dissolution of other minerals. Though in far lower abundances, CH_3COOH-extractable Al also increases with exposure age (Fig. 6), indicating that some non-carbonate minerals are dissolving in the acetic acid extraction. There is also a significant Na component (6% of cations by mass) in the CH_3COOH extraction (Table 1). This is unlikely to be natron or trona, which are H_2O soluble and would have come out in the previous extraction, but could represent Na-bearing sulphates (glauberite or mirabilite) whose kinetics did not allow for complete dissolution in the H_2O leach or non-carbonate minerals dissolving in the CH_3COOH extraction.

The most abundant elements in the HCl extraction (Fe and Al) show small increases with surface exposure age (Fig. 6). If these elements are interpreted as oxyhydroxides (i.e. Wiederhold et al., 2007), the gain in oxyhydroxide content represents an increase of 0.8 ± 0.2 wt% over the 1 Ma period (Table 1). However, there are also substantial gains in HCl extracted Ca and Mg, which are unlikely to source from oxyhydroxides. The Ca and Mg could represent carbonates that failed to dissolve in the CH_3COOH extraction, phosphate minerals such as apatite, or aluminosilicates such as zeolites or smectite. The increases with exposure age are nearly identical for Ca and Mg once normalized for atomic mass (Table 1), suggesting this could primarily represent dolomite dissolution.

The large, discontinuous change in grain size distribution at the Zone 3 - Zone 4 boundary (Fig. 3) is only weakly reflected in the relative mineral and chemical abundances of the <63 μm fraction. At the transition, the elemental abundances of Ca, Na, and Ti in the first five Zone 4 samples are slightly above those of the final two Zone 3 sampling points; Si is comparably lower (Fig. 4). These correspond to an increase in pyroxene and plagioclase (Fig. 5) and decreases in smectite, CH_3COOH-extracted Ca, and CH_3COOH-extracted Al (Figs. 5 and 6). This suggests a small, but detectable change in either source material that does not correlate with igneous clast abundance or in the processes that produce the chemical and mineral constituents of the <63 μm fraction across this boundary.

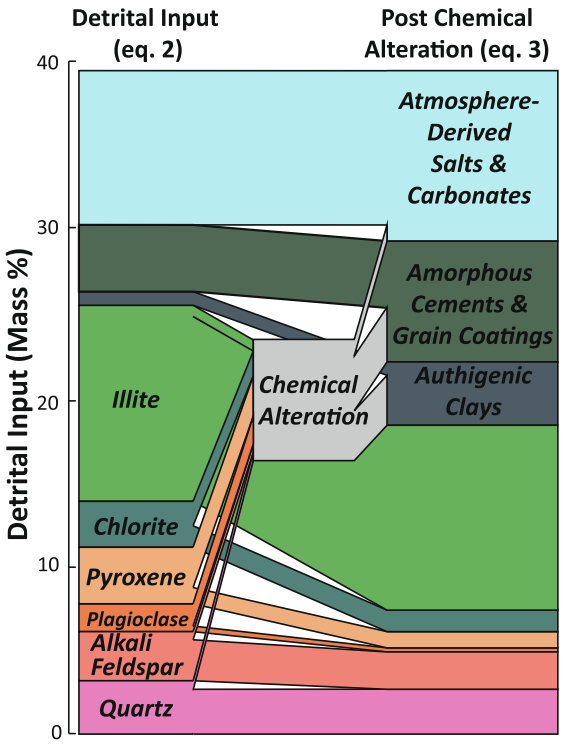

Fig. 10. A solution to the mass inputs as a percentage beyond initial mass and chemical alterations that explains the evolution of mineral and chemical abundance in the <63 μm fraction with time (Figs. 4-6). The left side shows the mineral input in addition to the <63 μm fraction's initial mass that solves for elemental composition after 500 ka of evolution via Eq. (2) (i.e. Fig. 4). Detrital input over the 500 ka period is calculated as 39% above the initial sediment mass. The right side accounts for leaching and alteration on the moraine surface in terms of the 500 ka of mineral abundance evolution via Eq. (3) (i.e. Fig. 5). This solution minimizes the mass input required; other solutions are found in Appendix C.

3.3. Clast Compositional Control on Chemistry and Mineralogy

To examine the influence of source material and subglacial processes on the composition of the moraine's surface, we normalize the composition of the <63 μm fraction for age and consider it as a function of the fraction of Ferrar Dolerite within the pebble and cobble clasts. Once exposure-age-normalized, LOI and Ca significantly increase with igneous clast abundance, whereas Si, Al, Fe, K, and Ti decrease (Fig. 7). Mg and Na do not show significant changes. Compared with the composition of the underlying rocks, few of the elements in the <63 μm fraction plot on a plausible mixing line between the composition of the sedimentary rocks and igneous rocks (Fig. 7). This is particularly striking for Fe, Mg, and Ca, in which the mafic igneous rocks are highly enriched, but the variation within sediments as a function of clast composition is minimal. The trendlines for Si, Mg, Ca, and K all intersect the mixing line at a value consistent with an ~20–30% contribution of igneous rock to the <63 μm fraction. Al, Ti, and LOI are consistently enriched above the mixing line; Na and Fe

Please cite this article in press as: Graly J. A., et al. Chemical weathering signatures at Mt. Achernar, Central Transantarctic Mountains II: Surface exposed sediments. *Geochim. Cosmochim. Acta* (2022), https://doi.org/10.1016/j.gca.2022.06.024

Table 2
Model Output (Complete solution range in Appendix C).

Detrital inputs to the <63 μm fraction	Bedrock Abundance (wt. %)	Clay Precipitation Allowed			Clay Precipitation Forbidden		
		Detrital Input	Proportion to Bedrock	Chemical Gain/ Loss	Detrital Input	Proportion to Bedrock	Chemical Gain/ Loss
Atmosphere	N/A	7.76	N/A	N/A	8.60	N/A	N/A
Leached Ca	N/A	0.95	N/A	0.39	1.30	N/A	0.53
Leached Mg	N/A	0.12	N/A	0.44	0.14	N/A	0.61
Leached Na	N/A	0.28	N/A	0.18	0.40	N/A	0.16
Quartz	26.35	3.14	0.38	−0.48	5.64	0.46	−0.40
Pyroxene	10.70	3.35	0.98	−2.38	4.67	0.95	−3.09
Alkali Feldspar	19.98	2.90	0.46	−0.68	4.46	0.48	−0.55
Plagioclase	9.57	1.65	0.54	−1.42	2.07	0.47	−1.48
Illite	11.76	11.59	3.11	−0.62	14.66	2.70	−0.42
Smectite	0.90	0.39	1.39	2.95	4.57	11.07	−0.30
Kaolinite	0.48	0.40	2.63	0.03	0.94	4.21	−0.29
Chlorite	1.44	2.72	5.95	−1.43	2.78	4.19	−1.14
Amorphous Si	7.14	0.26	0.11	1.99	0.23	0.07	3.55
Grain Cements	6.49	3.69	1.79	1.22	3.69	1.23	2.24

are consistently depleted. Significant increases with igneous cobble composition also occur for Mn, Zr, and Hf; P, Ba, Sr, Y, Cr, Zn, Ga, Ge, Rb, Ta, Pb, Th, U, and most of the rare earth elements show significant declines (Table 1).

Exposure-age-normalized mineral abundances show significant increases in smectite and amorphous Si and significant decreases in quartz and illite as a function of igneous clast composition (Fig. 8). Changes in the other analyzed minerals are not statistically significant (Table 1). As with the elemental compositions, most mineral abundances do not match the mixing lines between rock type compositions. Plagioclase and pyroxene are far below their abundance in the igneous rock, indicating that the abundance of these minerals in <63 μm fraction is not at all controlled by their abundance in the cobble and pebble fraction. Alkali feldspar does intersect the mixing trend, but the abundance of alkali feldspar at the intersection value is low enough to also suggest significant depletion compared with rock. All four clay minerals and amorphous Si are enriched in the <63 μm fraction.

Changes in exposure-age normalized sequential extraction data as a function of igneous clast abundance are statistically significant in a few cases (Fig. 9, Table 1). CH_3COOH-, HCl-, and NH_2OH-HCl-extracted Fe all decline with igneous clast abundance, as does NH_2OH-HCl-extracted Mg. CH_3COOH- and HCl-extracted Ca increase with igneous clast abundance. The mixing of sedimentary rock and igneous rock composition closely matches the trends for several of the extractions (i.e. all three Mg extracts and HCl-extracted Fe). However, for others, especially the Ca extractions, the data diverge significantly.

3.4. Physical and chemical inputs at the moraine surface

Using our fmincon modeling approach (Appendix A), we explain the observed changes in elemental composition (i.e. Figs. 4–6) over the 500 ka reference period by input to the <63 μm fraction of ~40% or more beyond its initial mass (Fig. 10, Table 2, Appendix C). This input mass consists of atmospheric deposition and detrital input of minerals or chemical leachates from disintegrating coarser grain size fractions. Approximately one quarter of the input is atmospheric salts or acids, one half is sedimentary-rock hosted clays (i.e. illite and chlorite) and intergranular cements, and one quarter is primary quartz, feldspar, and pyroxene found in both igneous and sedimentary rock types (Fig. 10). Relative to the composition of the underlying bedrock, secondary clays are strongly overrepresented and quartz and feldspar underrepresented in this detrital input (Table 2). This results in the declining fractional abundances of quartz and feldspar (Fig. 5) as proportionally fewer of these minerals enter the fine fraction. The increasing abundance of clays and amorphous cements implies an important role for physical friability in controlling the composition of detrital input.

Apart from physical inputs, weathering fluxes within the fine fraction were calculated via Eq. (3). Large losses of plagioclase, pyroxene and chlorite, and statistically insignificant losses of quartz and illite are implied (Fig. 10). The

Table 3
Weathering Products from Sequential Extractions vs Model Results.

Element	Build-up in extracted phases (Δ/Ma)	Modeled from weathering (clays)	Modeled from weathering (no clays)
Na	2.15 ± 0.18	2.32	2.49
Mg	1.12 ± 0.15	1.13	1.15
Ca	3.13 ± 0.4	2.39	2.44
Al	−0.05 ± 0.36	0.11	0.22
Fe	0.69 ± 0.42	0.92	0.86
H*	0.11 ± 0.01	0.12	0.13
Si**	−2.38 ± 2.09	−3.65	−3.64

* Assumed as initial component of carbonate, nitrate, and half of sulfate measured in H2O and Acetic acid leaches.
** Based on residual from XRD (not measured in extractions).

relative weathering rates (i.e. pyroxenes and plagioclase most easily weathered, etc.) are comparable to what is observed in temperate environments (e.g. White, 1995). The products of these weathering processes remain in the fine fraction, with the inferred losses in detrital mineral abundances approximately matching the gain in carbonate minerals, clay minerals, and amorphous material (Fig. 10, Table 3). Furthermore, the acid input from atmospheric deposition closely matches the acid needed to perform the inferred weathering (Table 3). Because of the scatter in the mineralogical data (Fig. 5), the loss values are uncertain. It is possible to model these mineral transformations without the formation of authigenic clay at this site by either taking a value from the lower end of the slope range for smectite or by positing much larger detrital input, including detrital input of authigenic clays from pre-weathered clasts (Table 2). Nevertheless, we think that our analytical model, which employs the best fit of the data and minimizes detrital input, is the most likely explanation of the moraine's chemical and mineralogical evolution with time (i.e. Figs. 4–6).

3.5. Total Chemical Fluxes

Both the thickness of moraine sediments and the ratio between depth-integrated and surface concentrations of salts and carbonates follow power law relationships with surface age (Fig. 11). Following Eq. (4), the total relationship between time in ka (t) and the inventory in g·cm^{-2} (I) of a species X in wt.% can be described by:

$$I = \rho \cdot \frac{X_i + tF_X}{1 + t\sum_{j=1}^{n} F_j} \cdot D \cdot C \cdot t^{(D_{exp}+C_{exp})} \quad (5)$$

where ρ is effective density in g·cm^{-3} at depth accounting for the fact that only the <63 μm fraction is measured, D and D_{exp} are the power-law terms for deriving moraine thickness (cm) from time (ka), and C and C_{exp} are power-law terms of the relationship between surface concentration of X and its average concentration at depth as a fuction of time. The ρ term is unconstrained both here and in Scarrow and others (2014) work, as density was not directly measured, and silt and clay abundance do not have a simple relationship to age (Fig. 3). Density of Antarctic tills elsewhere is ~1.5 g·cm^{-3}. Clays and silts are ~40% of sediment mass on average (Fig. 3), so ρ is estimated at ~0.6 g·cm^{-3}, though the lack of further empirical quantification makes this term uncertain. The terms D and C are derived from power law correlations for salt and carbonate mineral species (Fig. 11, Table 4). $\sum_{j=1}^{n} F_j$ is set at 0.39/500 from the minimizing convolution model, solved for 500 ka of exposure (Table 2, Appendix C). X_i and X_{flux} derive from the linear regression values at 500 ka for the salts in question (Table 1).

For all the salt species including sulfate, chloride, nitrate, H_2O-extracted Na, H_2O-extracted Ca, and H_2O-extracted Mg, Eq. (5) very closely approximates linearity, allowing us to postulate constant fallout or leaching of these elements (Table 4). The average fallout rates of sulfate, nitrate, and chloride to the moraine are 4.1 ± 2.7, 3.8 ± 2.5, and 2.8 ± 1.5 mg·m^{-2}·a^{-1}, respectively (Appendix D). These are comparable to Pleistocene flux values preserved in ice cores in the ice sheet interior (Legrand et al., 1988; Watanabe et al., 2003; Wolff et al., 2010).

The cation composition of snow and ice at Vostok is, averaged over the glacial interglacial cycle, ~40% acid (i.e. H^+), 37% Na, 12% Ca and 11% Mg by molar equivalents (Legrand et al., 1988). Including the salts accumulated at depth (Fig. 11), the water-soluble portion of the <63 μm fraction is 69% Na, 23% Ca and 8% Mg by molar equivalents. This indicates that the acidic portion of the atmospheric fallout has exchanged for Na and Ca, with little or no extraction of any other cation.

Because the average concentration of carbon at depth increases faster than the concentration at the surface (Fig. 11E), we cannot expect a linear fit for C accumulation in the moraine. The average modeled rate is 50.6 ± 24.6 m g·m^{-2}·a^{-1} CO_3 buildup (which is equivalent to 37 mg·m^{-2}·a^{-1} CO_2 drawdown). But this rate varies from 3 mg·m^{-2}·a^{-1} CO_3 buildup in the youngest soils to 65 mg·m^{-2}·a^{-1} after 1 Ma of surface exposure (Appendix D). These values far exceed that of the salts, whose concentrations at depth are lower than at the surface.

Excluding atmosphere-derived sea salt, our model shows ~32 mg·m^{-2}·a^{-1} of leached cations accumulating in salts and carbonates. Assuming a ratio of Ca to Mg carbonate comparable to that found at the surface, the leached material would comprise of 77% Ca, 17% Mg and 6% Na. The remainder of the chemically weathered moraine material accumulates as amorphous material or perhaps as authigenic zeolites and clays.

Please cite this article in press as: Graly J. A., et al. Chemical weathering signatures at Mt. Achernar, Central Transantarctic Mountains II: Surface exposed sediments. *Geochim. Cosmochim. Acta* (2022), https://doi.org/10.1016/j.gca.2022.06.024

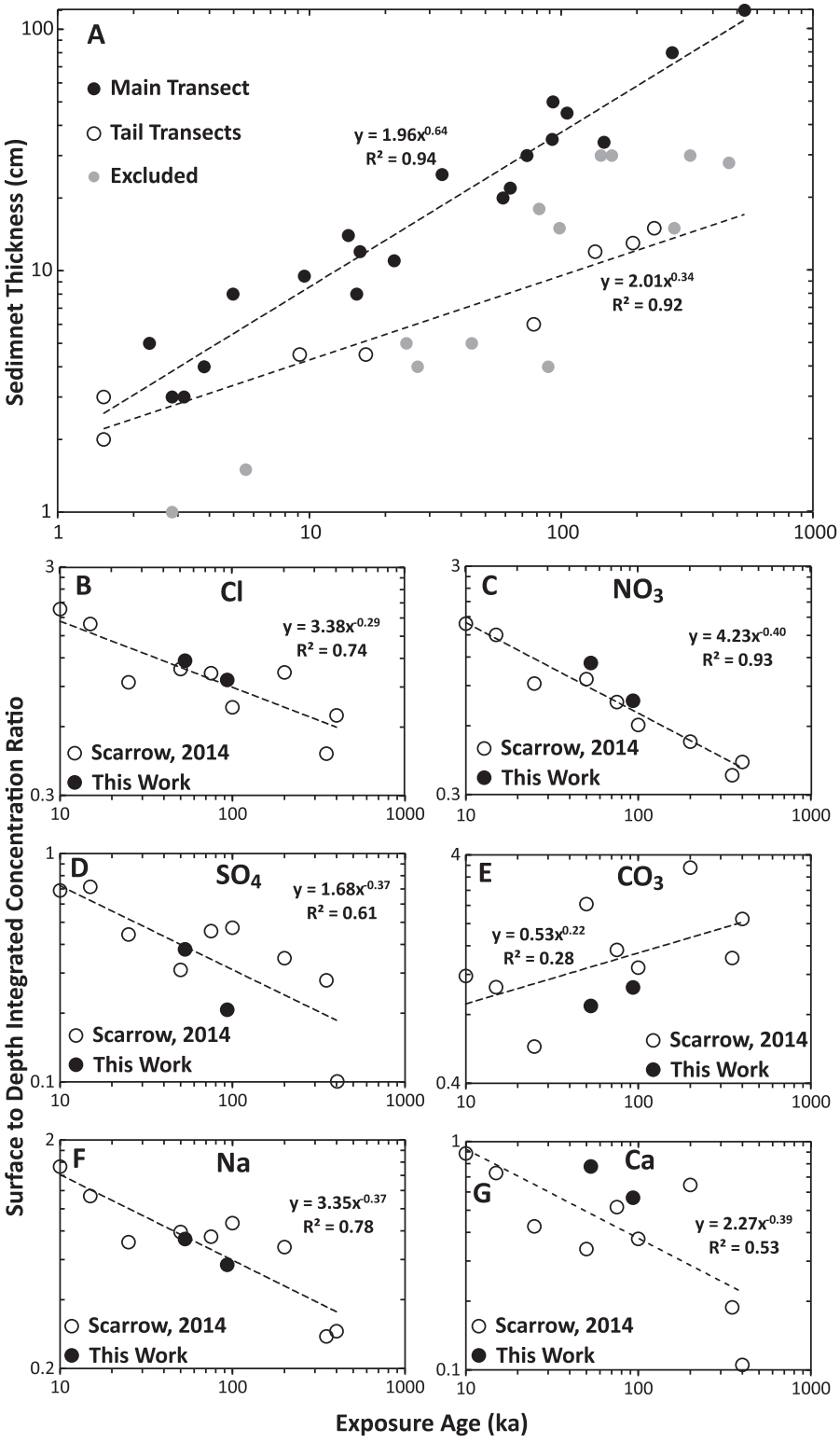

Fig. 11. Empirical trends employed to convert surface concentrations into a total inventory of salt and carbonate ions in the soil profile. A shows a power law relationship between sediment thickness and exposure age. The main transect plots on a distinct trend compared with the tail transects, indicating either that sediment accumulates more slowly in the tail or perhaps that the age model calibrated on the main transect does not accurately apply to the tail. Excluded values are either off transect, off moraine ridges, or indicate places where the penetration was unlikely to have reached ice at depth. B-G compare surface exposure age with the ratio between concentration in surface sediments and an estimated average concentration at depth. Scarrow et al. (2014) ages are estimated from total salt concentrations. Data are presented for water extracted chloride (B), nitrate (C), sulfate (D), Na (F), and Ca (G). Carbonate (E) is calculated as the anion balancing acetic acid extracted Ca and Mg for "This Work" and from total carbon for Scarrow et al., 2014.

Please cite this article in press as: Graly J. A., et al. Chemical weathering signatures at Mt. Achernar, Central Transantarctic Mountains II: Surface exposed sediments. *Geochim. Cosmochim. Acta* (2022), https://doi.org/10.1016/j.gca.2022.06.024

Table 4
Eq. (5) inputs and results.

Analyte	Initial (wt. %)	Linear Flux @ 500 ka (wt.%)	D Term	D Exp Term	C Term	C Exp Term	Net Flux @ 500 ka mg·m^{-2}·a^{-1}	Instant Flux @ 500 ka mg·m^{-2}·a^{-1}	Linear Flux (1 Ma) mg·m^{-2}·a^{-1}	R^2 of Linear Trend
Carbonate	1.00	1.37	1.6	0.69	0.67	0.16	35.6	50.6	51.1	0.977
Chloride	0.00	0.29	1.6	0.69	2.44	−0.20	2.8	3.4	3.2	0.997
Nitrate	0.08	0.55	1.6	0.69	2.08	−0.23	3.8	4.3	4.2	0.998
Sulfate	0.36	1.99	1.6	0.69	1.65	−0.39	4.1	4.0	4.1	0.999
Na H_2O	0.06	0.79	1.6	0.69	7.94	−0.49	4.1	3.7	3.7	0.996
Ca H_2O	0.12	0.39	1.6	0.69	2.49	−0.38	1.3	1.2	1.3	0.999
Mg H_2O	0.01	0.07	1.6	0.69	0.99	−0.21	0.3	0.3	0.3	0.999

4. DISCUSSION

Our analysis finds significant changes in moraine composition both as a function of exposure age (Figs. 4–6, 10, 11) and clast composition (Figs. 7–9). The former relates to processes that occur at the moraine's surface; the latter to either bedrock composition or processes altering clast abundance in the subglacial environment. In both subglacial and surface contexts, physical and chemical processes are shaping the chemical elements and minerals that comprise the moraine's surface sediments.

4.1. Moraine Composition as a Function of Surface Exposure

Mt. Achernar Moraine is a nearly waterless environment in which once sediment emerges from ice, only the atmosphere is capable of moving material to and from the moraine surface and vapor phases play a dominant role in formation of salts at depth (Graly et al., 2018b). Below the influence of wind deflation, chemically leached materials are not removed from the system. An element that is chemically leached from the fine fraction remains in the fine fraction as a salt, in carbonate minerals, or in amorphous phases. Gains in elemental abundance within the fine fraction must either reflect atmospheric deposition of that element, selective comminution of minerals containing that element into the fine fraction by physical processes, or leaching of that element from a coarser fraction into a mineral or amorphous phase of the fine fraction. In this setting, haloclasty (salt shattering), wind abrasion (including abrasion by driven snow), and thermal stress are the major grain size reducing processes (Lamp et al., 2017; Matsuoka et al., 1996). In summary, this amounts to five broad chemical and physical mechanisms that affect the chemical and mineralogical composition of the <63 μm fraction with surface exposure: (1) Dry fallout of salts from atmospheric sources (i.e. sea spray and/or products of aerosol particulate chemistry); (2) Dry deposition of acidic aerosols (i.e. N_2O_5, SO_3), which hydrate to nitric and sulfuric acid and attack the mineral structures of the substrate, forming salts and possibly other weathering products (i.e. oxides and clays); (3) Drawdown of atmospheric gases into hydrous acids (especially, H_2CO_3) which, like acidic aerosols, attack the mineral substrate; (4) Physical erosion of material from the coarser fraction into the fine fraction; (5) Dust deposition or winnowing. Our model of chemical and mineralogical change at Mt. Achernar moraine (i.e. Fig. 10) combines mechanisms 1–4, but does not consider mechanism 5, which we assume to be minimal due to our sampling strategy of collecting material from below the influence of wind.

A secondary atmospheric source of carbonate, nitrate, and sulfate is strongly suggested by stable isotopes elsewhere in the Transantarctic Mountains (Diaz et al., 2020). The formation of sulfuric or nitric acid from atmospheric aerosols (Mechanism 2) and of carbonic acid from atmospheric CO_2 (Mechanism 3) require conditions where a gas or aerosol particle interacts with H_2O to form an acid. This acid subsequently exchanges H^+ for cations from minerals surfaces to form salts and carbonates (e.g. Jackson et al., 2016). Under the intense cold and aridity typical of

the Mt. Achernar Moraine setting, H_2O exists as ice or in vapor phase, either from sublimating snow at the surface of the moraine or from sublimating ice at the moraine's base. Under rare conditions surface snow could melt, creating ephemeral wetting of the moraine surface. Experiments conducted with the Martian context in mind have shown that carbonate minerals can form rapidly from a frost coating and even without any kind of wetting (Booth and Kieffer, 1978). The vapor from sublimating snow may be sufficient to produce aqueous acids. The accumulation of carbonate minerals at the base of the profile suggests a strong role for the ablating ice in supplying vapor for the formation of H_2CO_3 (Foley et al., 2006), whereas the diffusion of aerosol vapors (i.e. N_2O_5, SO_3) to the base may be limited by their low vapor pressures at the relevant temperatures (Graly et al., 2018b).

The rate of carbon sequestration in the surface sediments of Mt. Achernar Moraine (i.e. 37 $mg{\cdot}m^{-2}{\cdot}a^{-1}$ CO_2 drawdown) is well below the range of values found in warm desert soils: 1000–3500 $mg{\cdot}m^{-2}{\cdot}a^{-1}$ (e.g. Schlesinger, 1985). It is also more than an order of magnitude below the 380–1600 $mg{\cdot}m^{-2}{\cdot}a^{-1}$ estimated for CO_2 drawdown in the subglacial environment inferred from the comparisons of freshly emerging sediments to rock at Mt. Achernar Moraine (Graly et al., 2020). The role of climate in pedogenic carbonate development in desert soils has been debated, with some studies arguing that mean annual precipitation has a controlling role in pedogenic carbonate development (e.g. Landi et al., 2003) and others failing to observe any such an effect (e.g. Quade et al., 1989). Our work here provides an end member to this debate, by illustrating substantial pedogenic carbonate development in a region where liquid water is absent but at a far lower rate than documented in water-bearing environments. Vapor phase processes could be important to pedogenic carbonate development in other regions as well.

Beyond salts and carbonate minerals, weathering on the moraine surface can create a variety of products: oxides, amorphous material, zeolites, and clay minerals, depending on the chemical pathway. Larger clasts within Antarctic settings often exhibit oxidation rind development, facilitated by cation exchange on mineral surfaces (Salvatore et al., 2013). The oxidation rind leaching may be the major source of cations that we infer to be fluxed from the coarser fraction into the finer fraction in our model of moraine evolution (Table 2). The oxidation and subsequent friability of Fe-bearing minerals within these rinds could also help explain the relatively large role of pyroxenes and chlorite in both physical and chemical weathering (Fig. 10, Table 2).

Precipitation of amorphous constituents from subaerial weathering of glacial sediments has been observed in a number of settings, including Taylor Valley (Quinn et al., 2020), maritime Antarctica (Mendonça et al., 2013), and temperate proglacial environments (Rutledge et al., 2018). We find relatively comparable roles for physical and chemical processes in producing amorphous products in this setting, with detrital process (i.e. input from grain cements in sedimentary rocks) accounting for approximately half the gain in amorphous content (Fig. 10). Furthermore, the initial amorphous content of the sediment is high – likely due to weathering in the subglacial environment (Graly et al., 2020). The input of new amorphous material (whether detrital or chemical) is input at a similar rate as other material (salts, etc.); thus amorphous Si, extractable Fe, and extractable Al either stay approximately constant, slightly increase, or slightly decline with exposure age (Figs. 5 and 6).

Tills of the Sirius Formation contain substantial abundances of authigenic zeolites (Dickinson and Grapes, 1997). An increase with exposure age in X-ray diffraction detectable laumontite (Fig. 5) suggests authigenic zeolite formation may also occur at Mt. Achernar Moraine. Zeolites are likely to be HCl soluble (Hartman and Fogler, 2007) and probably contribute to the increase in HCl-soluble Ca and Al with exposure age (Fig. 6).

Authigenic clay formation in non-glaciated soils of Antarctica is suggested in many locations in the Transantarctic Mountains, though in small abundances (<1%) (Vennum and Nejedly, 1990). Larger abundances of clay minerals have been found in glacial soils of maritime Antarctica. And though some of these clays may be detrital in origin (Jeong and Yoon, 2001), kaolinite and smectites do form directly from plagioclase and pyroxene in soil environments (Schaefer et al., 2008; Simas et al., 2006). We cannot definitively argue for clay formation in the surface environment here, as the small amounts of these clay minerals were detected in bedrock clasts and could be surficial detrital inputs to the <63 μm fraction (Table 2). But the low abundance of smectite and kaolinite in the underlying rock (Graly et al., 2020) and the parsimony of modeling clay formation (Fig. 10) makes us believe that neoformation of these minerals on the surface environment is likely.

The dominance of fine material (clays and amorphous grain coatings) in the physical detrital input (Fig. 10) is also observed in a wide range of interior Antarctic settings (Bockheim, 1997). Our innovation here is to show how these physical and chemical processes combine. The physical input of pyroxenes, plagioclase, and chlorite provides the base material that is weathered by carbonic, sulfuric, and nitric acids to form carbonate minerals and non-sea salts, along with amorphous material, zeolites, and authigenic clays.

4.2. Zonal Transitions and Sediment Source

At each transition between the moraine's geomorphic zones, we observe younger, coarser sediment in the newly emerging zone (Fig. 3). Zones 4 and 5 plot on separate grain size – exposure age trendlines from Zones 1–3. This implies they had an initially coarser grain size distribution and only reached a comparable abundance of silt and clay sized particles after several hundred thousand years of additional physical erosion. The notion of two distinct regimes of sediment generation at Mt. Achernar Moraine is strongly supported by ground penetrating radar results, which show discrete bands of subglacial debris emerging along the surface for Zones 1–3 but show much higher debris content and a possible topographic shelf beneath Zone 4 (Kassab et al., 2020). This may reflect a switch in debris origin from a locally derived source in Zone 4 to a more distant source

Please cite this article in press as: Graly J. A., et al. Chemical weathering signatures at Mt. Achernar, Central Transantarctic Mountains II: Surface exposed sediments. *Geochim. Cosmochim. Acta* (2022), https://doi.org/10.1016/j.gca.2022.06.024

in Zones 1–3 (Bader et al., 2017), with transport distance controlling variation in the production of fine grained subglacial material. The minor, but detectable shift towards a less chemically weathered <63 μm fraction in Zone 4 (Figs. 4–6) may also reflect this transport distance control.

4.3. Moraine Composition as a Function of Subglacial Processes

Variation in the composition of the <63 μm fraction as a function of clast composition shows an almost complete lack of correspondence to mixing lines between rock type end members (Figs. 7–9). This suggests that the variation does not reflect the underlying geology but instead represents variation in the preservation of pebble and cobble sized material between igneous and sedimentary rock. The sedimentary rocks at Mt. Achernar Moraine consist of contact metamorphosed sandstones, siltstones, and shales (Bader et al., 2017). Sedimentary and metasedimentary rocks are found to be more friable than igneous rocks in laboratory tests and in other glaciological environments (Crompton and Flowers, 2016; Lee and Rutter, 2004), suggesting the sedimentary and metasedimentary rocks found at Mt. Achernar Moraine may be far more friable than the igneous Ferrar dolerite. Therefore, the portions of the moraine with higher abundance of igneous rocks likely reflect areas of more effective crushing of rock material in the subglacial environment, disproportionately destroying the sedimentary and metasedimentary cobble and pebble clasts.

Our earlier analysis of element balance in the most freshly emerging sediments of Zone 1 suggests a ~70% contribution of sedimentary rock in samples where igneous clasts account for 64% of rock composition (Graly et al., 2020). A similar contribution of sedimentary rock across the entire moraine is implied here in the intersection of the Si, Mg, and Ca trendlines with the endmember mixing line at around 30% igneous clasts (Fig. 7). The implication is that the samples with few igneous clasts (Zones 2 and 3 and bands in Zone 4) preserve a cobble and pebble composition reflective of the underlying rock, whereas Zones 1, 5, and much of Zone 4 have lost their sedimentary clasts to physical erosion. It is likely that this physical erosion took place in the subglacial environment, as the surface environments are otherwise comparable. It is also possible that some of these zones may have had greater abundance of igneous rock initially, but the continued presence of minerals such as illite that source exclusively from sedimentary and metasedimentary rocks (Fig. 8) and the lack of any increase in Fe or Mg (Fig. 7) in these setting implies that this underlying compositional signal is small.

Samples with greater abundance of igneous clasts show greater abundance of LOI, amorphous Si, smectite, kaolinite, and CH_3COOH- and HCl-extracted Ca (Figs. 7–9). These are likely to be primarily chemical weathering products (or the components thereof), as their abundances in the underlying rock are low. This suggests that the physical subglacial processes responsible for the loss of sedimentary rock clasts occurs in the same location as intensified subglacial chemical weathering. It may be that physical weathering creates the fresh mineral surfaces prone to chemical weathering. Or that a common variable, such as meltwater abundance, promotes both physical and chemical weathering in the subglacial environment (perhaps through enhanced sliding and oxygen availability, respectively). The highly zonal nature of igneous clast distribution on the moraine is suggestive of distinct blocks of subglacial debris, each capturing its own subglacial regime (Bader et al., 2017; Kassab et al., 2020).

The gain in authigenic weathering products in the <63 μm fraction with igneous pebble and cobble clast abundance comes primarily through proportional declines in quartz and illite (Fig. 8). Because Si, Al, and K decline commensurately (Fig. 7), quartz and illite are unlikely to be major chemical reactants. Instead, the data are best explained by igneous clast rich samples supplying higher quantities of plagioclase and pyroxene to the <63 μm fraction, which in turn are the primary chemical reactants in the subglacial environment – forming the smectite and amorphous Si that increase with abundance of igneous clasts (Fig. 8). This implies that the subglacial regions with more intense physical and chemical weathering have proportionally greater input from igneous rock into the <63 μm fraction, possibly from greater physical deterioration of igneous rock in a water-rich environment (e.g. Anderson, 2005; Graly et al., 2018a).

The chemical weathering products formed in the subglacial environment are similar to those formed in the surface environment. In both settings, clays, carbonates, and amorphous material are the primary authigenic mineral products, with plagioclase and pyroxene disproportionately comprising the reactants. The compositional difference between the surface and subglacial environments comes from physical input to the <63 μm fraction. In the subglacial environment, mineral input is more proportional to bedrock composition (Graly et al., 2020), whereas bedrock-derived clays and grain cements are strongly overrepresented in the mineral input on the surface environment. (Fig. 10, Table 2). The continuity between the environments suggests a fundamental control of source material on geochemistry even in conditions that differ dramatically in terms of liquid water, atmospheric contact, and temperature.

5. CONCLUSIONS

Mt. Achernar Moraine provides a well-dated record of emerging subglacial sediments and their subsequent alteration in a cold, dry surface environment. Along an ~1 Ma transect, there are significant changes in the relative abundances of mineral species and chemical elements within the <63 μm fraction. The variation can be decomposed into two parts: (1) a subglacial processes signal traced by the lack of preservation of friable sedimentary rock in the pebble fraction, and (2) a surface exposure age signal traced by a boron accumulation proxy and cosmogenic dating. The subglacial processes signal shows high input of clays and amorphous Si where active subglacial processes breakdown sedimentary rock, suggesting a link between physical and chemical processes in the subglacial environ-

Please cite this article in press as: Graly J. A., et al. Chemical weathering signatures at Mt. Achernar, Central Transantarctic Mountains II: Surface exposed sediments. *Geochim. Cosmochim. Acta* (2022), https://doi.org/10.1016/j.gca.2022.06.024

ment. The surface exposure age signal shows large detrital inputs of clays and grain cements from sedimentary rock and buildup of atmosphere-derived salts. Contrastingly, detrital input of feldspars and quartz is relatively small compared with their abundance in the cobble and pebble fraction. The differences between the initial composition of the moraine's sediments and the composition of this detrital fraction result in changes to the mineral composition of the <63 μm fraction on the moraine's surface as a function of time.

Chemical weathering on the moraine surface is driven by acids formed from aerosols and carbonic acid derived from atmospheric CO_2. The minimal occurrence of liquid water in an environment where loss of ice and snow is almost entirely driven by sublimation does not inhibit the formation of these acids, suggesting formation of aqueous acids as these vapors condense on mineral surfaces. Our limited data from lower positions in the till soil profile suggest that carbonic acid and its consequent carbonate minerals form at higher rates at depth than at the surface. This implies increasing rates of CO_2 drawdown as the moraine thickens, which may exceed 50 $mg{\cdot}m^2{\cdot}a^{-1}$ in the oldest parts of the moraine. Cold and aridity do not prevent weathering entirely. Vapor chemistry and physical disintegration have substantial effects over hundred thousand-year timescales at Mt. Achernar Moraine.

The mafic minerals from the Ferrar dolerite (plagioclase and pyroxene) are the primary targets of subglacial and subaerial chemical weathering at Mt. Achernar Moraine. The geochemical reactions acting on these mafic minerals form smectite and kaolinite clays, amorphous Si, and zeolites in both settings. However, authigenic clay and amorphous Si are more strongly linked to subglacial weathering and zeolite formation to subaerial weathering. The subglacial weathering regime is more intensive, forming new minerals at an order of magnitude higher rates than at the moraine surface. Despite the low rates, chemical alteration on the surface environment still has an appreciable impact on authigenic mineral formation and drawdown of atmospheric gases.

DECLARATION OF COMPETING INTEREST

The authors declare that they have no known competing financial interests or personal relationships that could have appeared to influence the work reported in this paper.

ACKNOWLEDGEMENTS

This work was supported by National Science Foundation Antarctic grants PLR-1744879, PLR-1443433, PLR-1443213, ANT-0944578 and ANT-0944475, by an Indiana University Collaborative Research Grant, and by funding from the IUPUI Office of the Vice Chancellor for Research. The US Antarctic Program, Kenn Borek Air, Ltd., and field team members from the 2010 and 2015 seasons are gratefully acknowledged for field support. T. Kennedy assisted with magnetic susceptibility analyses. H. Johnston assisted with particle size analyses. S. Cox and S. Olund assisted with the sequential extraction analyses. Reviews by J. Compton and by an anonymous reviewer, along with editing by L. Jin and J. Catalano, were helpful in improving the manuscript. We would like to acknowledge the Integrated Nanosystems Development Institute (INDI) for use of their Bruker D8 Discover X-Ray Diffraction Instrument, which was awarded through NSF grant MRI-1429241.

APPENDIX A. SUPPLEMENTARY MATERIAL

Supplementary material to this article can be found online at https://doi.org/10.1016/j.gca.2022.06.024.

REFERENCES

Anderson S. P. (2005) Glaciers show direct linkage between erosion rate and chemical weathering fluxes. *Geomorphology* **67**, 147–157.

Bader N. A., Licht K. J., Kaplan M. R., Kassab C. and Winckler G. (2017) East Antarctic ice sheet stability recorded in a high-elevation ice-cored moraine. *Quat. Sci. Rev.* **159**, 88–102.

Bockheim J. G. (1990) Soil development rates in the Transantarctic Mountains. *Geoderma* **47**, 59–77.

Bockheim J. G. (1997) Properties and classification of cold desert soils from Antarctica. *Soil Sci. Soc. Am. J.* **61**, 224–231.

Booth M. C. and Kieffer H. H. (1978) Carbonate formation in marslike environments. *J. Geophys. Res.* **83**, 1809–1815.

Claridge G. and Campbell I. (1984) Mineral transformation during the weathering of dolerite under cold arid conditions in Antarctica. *N. Z. J. Geol. Geophys.* **27**, 537–545.

Comiso J. C. (2000) Variability and trends in Antarctic surface temperatures from in situ and satellite infrared measurements. *J. Clim.* **13**, 1674–1696.

Crompton J. W. and Flowers G. E. (2016) Correlations of suspended sediment size with bedrock lithology and glacier dynamics. *Ann. Glaciol.* **57**, 142–150.

Diaz M. A., Li J., Michalski G., Darrah T. H., Adams B. J., Wall D. H., Hogg I. D., Fierer N., Welch S. A., Gardner C. B. and Lyons W. B. (2020) Stable Isotopes of Nitrate, Sulfate, and Carbonate in Soils From the Transantarctic Mountains, Antarctica: A Record of Atmospheric Deposition and Chemical Weathering. *Front. Earth Sci.* **8**.

Dickinson W. W. and Grapes R. H. (1997) Authigenic chabazite and implications for weathering in Sirius Group diamictite, Table Mountain, dry valleys, Antarctica. *J. Sediment. Res.* **67**, 815–820.

Faure G. and Mensing T. M. (2010) *The Transantarctic Mountains: Rocks, ice, meteorites and water*. Springer Science & Business Media.

Foley K. K., Lyons W. B., Barrett J. E. and Virginia R. A. (2006) Pedogenic carbonate distribution within glacial till in Taylor Valley, southern Victoria Land, Antarctica. *Special Pap.-Geol. Soc. Am.* **416**, 89–103.

Graly J. A., Humphrey N. F. and Licht K. J. (2018a) Two Metrics Describing the Causes of Seasonal and Spatial Changes in Subglacial Aqueous Chemistry. *Front. Earth Sci.* **6**.

Graly J. A., Licht K. J., Bader N. A. and Bish D. L. (2020) Chemical weathering signatures from Mt. Achernar Moraine, Central Transantarctic Mountains I: Subglacial sediments compared to underlying rock. *Geochim. Cosmochim. Acta* **283**, 149–166.

Graly J. A., Licht K. J., Drushel G. K. and Kaplan M. R. (2018b) Polar desert chronologies through quantitative measurements of salt accumulation. *Geology* **46**, 351–354.

Graly J. A., Licht K. J., Kassab C. M., Bird B. W. and Kaplan M. R. (2018c) Warm-based basal sediment entrainment and far-field Pleistocene origin evidenced in central Transantarctic blue

ice through stable isotopes and internal structures. *J. Glaciol.* **64**, 185–196.

Hagen E. H. (1995) *A geochemical and petrological investigation of meteorite ablation products in till and ice of Antarctica*. The Ohio State University, p. 525.

Hartman R. L. and Fogler H. S. (2007) Understanding the dissolution of zeolites. *Langmuir* **23**, 5477–5484.

Jackson A., Davila A. F., Böhlke J. K., Sturchio N. C., Sevanthi R., Estrada N., Brundrett M., Lacelle D., McKay C. P. and Poghosyan A. (2016) Deposition, accumulation, and alteration of Cl^-, NO_3^-, ClO_4^- and ClO_3^- salts in a hyper-arid polar environment: Mass balance and isotopic constraints. *Geochim. Cosmochim. Acta* **182**, 197–215.

Jeong G. and Yoon H. (2001) The origin of clay minerals in soils of King George Island, South Shetland Islands, West Antarctica, and its implications for the clay-mineral compositions of marine sediments. *J. Sediment. Res.* **71**, 833–842.

Kaplan M. R., Licht K. J., Winckler G., Schaefer J. M., Bader N., Mathieson C., Roberts M., Kassab C. M., Schwartz R. and Graly J. A. (2017) Mid-Late Pleistocene stability of the central East Antarctic Ice Sheet at the head of Law Glacier. *Geology* **45**, 963–966.

Kassab C. M., Licht K. J., Petersson R., Lindbäck K., Graly J. A. and Kaplan M. R. (2020) Formation and evolution of an extensive blue ice moraine in central Transantarctic Mountains, Antarctica. *J. Glaciol.* **66**, 49–60.

Lamp J., Marchant D., Mackay S. and Head J. (2017) Thermal stress weathering and the spalling of Antarctic rocks. *J. Geophys. Res. Earth Surf.* **122**, 3–24.

Landi A., Mermut A. and Anderson D. (2003) Origin and rate of pedogenic carbonate accumulation in Saskatchewan soils, Canada. *Geoderma* **117**, 143–156.

Lee A. and Rutter E. (2004) Experimental rock-on-rock frictional wear: Application to subglacial abrasion. *J. Geophys. Res. Solid Earth* **109**, B09202.

Legrand M. and Mayewski P. (1997) Glaciochemistry of polar ice cores: A review. *Rev. Geophys.* **35**, 219–243.

Legrand M. R., Lorius C., Barkov N. I. and Petrov V. N. (1988) Vostok (antarctica) ice core: Atmospheric chemistry changes over the last climatic cycle (160,000 years). *Antmos. Environ.* **22**, 317–331.

Matsuoka N., Moriwaki K. and Hirakawa K. (1996) Field experiments on physical weathering and wind erosion in an Antarctic cold desert. *Earth Surf. Proc. Land.* **21**, 687–699.

Mayewski P. A., Lyons W. B., Zielinski G. A., Twickler M. S., Whitlow S. I., Dibb J. E., Grootes P., Taylor K., Whung P. and Fosberry L. (1995) *An ice-core-based*. Late Holocene history for the Transantarctic Mountains, Antarctica.

Mayewski P. A., Twickler M. S., Lyons W. B., Spencer M. J., Meese D. A., Gow A. J., Grootes P., Sowers T., Watson M. S. and Saltzman E. (1990) The Dominion Range ice core, Queen Maud Mountains, Antarctica-General site and core characteristics with implications. *J. Glaciol.* **36**, 11–16.

Mendonça T., Melo V. F., Schaefer C. E. G., Simas F. N. and Michel R. F. (2013) Clay mineralogy of gelic soils from the Fildes Peninsula, maritime Antarctica. *Soil Sci. Soc. Am. J.* **77**, 1842–1851.

Nesbitt H. W. and Young G. M. (1982) Early Proterozoic climate and plate motions inferred from major element chemistry of lutites. *Nature* **299**, 715–717.

Quade J., Cerling T. E. and Bowman J. R. (1989) Systematic variations in the carbon and oxygen isotopic composition of pedogenic carbonate along elevation transects in the southern Great Basin, United States. *Geol. Soc. Am. Bull.* **101**, 464–475.

Quinn, J., Graff, T., and Ming, D. (2020) X-ray Amorphous Components of Antarctica Dry Valley Soils: Weathering Implications for Mars.

Rutledge A., Horgan B., Havig J., Rampe E., Scudder N. and Hamilton T. (2018) Silica Dissolution and Precipitation in Glaciated Volcanic Environments and Implications for Mars. *Geophys. Res. Lett.* **45**, 7371–7381.

Salvatore M., Mustard J., Head J., Cooper R., Marchant D. and Wyatt M. (2013) Development of alteration rinds by oxidative weathering processes in Beacon Valley, Antarctica, and implications for Mars. *Geochim. Cosmochim. Acta* **115**, 137–161.

Scarrow J. W., Balks M. R. and Almond P. C. (2014) Three soil chronosequences in recessional glacial deposits near the polar plateau, in the Central Transantarctic Mountains, Antarctica. *Antarct. Sci.* **26**, 573–583.

Schaefer C. E. G., Simas F. N., Gilkes R. J., Mathison C., da Costa L. M. and Albuquerque M. A. (2008) Micromorphology and microchemistry of selected Cryosols from maritime Antarctica. *Geoderma* **144**, 104–115.

Schlesinger W. H. (1985) The formation of caliche in soils of the Mojave Desert, California. *Geochim. Cosmochim. Acta* **49**, 57–66.

Simas F. N., Schaefer C. E. G., Melo V. F., Guerra M. B., Saunders M. and Gilkes R. J. (2006) Clay-sized minerals in permafrost-affected soils (Cryosols) from King George Island, Antarctica. *Clays Clay Miner.* **54**, 721–736.

Tessier A., Campbell P. G. C. and Bisson M. (1979) Sequential extraction procedure for the speciation of particulate trace metals. *Anal. Chem.* **51**, 844–851.

Ure A. M. and Davidson C. M. (2002) Chemical speciation in soils and related materials by selective chemical extraction. In *Chemical Speciation in the Environment* (eds. A. M. Ure and C. M. Davidson), Second Edition. Blackwell.

Van Wessem J., Reijmer C., Morlighem M., Mouginot J., Rignot E., Medley B., Joughin I., Wouters B., Depoorter M. and Bamber J. (2014) Improved representation of East Antarctic surface mass balance in a regional atmospheric climate model. *J. Glaciol.* **60**, 761–770.

Vennum W. R. and Nejedly J. W. (1990) Clay mineralogy of soils developed on weathered igneous rocks, West Antarctica. *N. Z. J. Geol. Geophys.* **33**, 579–584.

Watanabe, O., Kamiyama, K., Motoyama, H., Fujii, Y., Igarashi, M., Furukawa, T., Goto-Azuma, K., Saito, T., Kanamori, S., and Kanamori, N. (2003) General tendencies of stable isotopes and major chemical constituents of the Dome Fuji deep ice core.

White A. F. (1995) Chemical weathering rates of silicate minerals in soils. *Rev. Mineral. Chem. Weather. Rates Silicate Miner.*, 407–461.

Wiederhold J. G., Teutsch N., Kraemer S. M., Halliday A. N. and Kretzschmar R. (2007) Iron isotope fractionation in oxic soils by mineral weathering and podzolization. *Geochim. Cosmochim. Acta* **71**, 5821–5833.

Wolff E., Barbante C., Becagli S., Bigler M., Boutron C., Castellano E., DeAngelis M., Federer U., Fischer H. and Fundel F. (2010) Changes in environment over the last 800,000 years from chemical analysis of the EPICA Dome C ice core. *Quat. Sci. Rev.* **29**, 285–295.

Associate editor: Lixin Jin